European Journal of Mechanics / A Solids 119 (2026) 106194

Contents lists available at ScienceDirect

European Journal of Mechanics / A Solids

journal homepage: www.elsevier.com/locate/ejmsol

Full length article

Longitudinal waves in two-dimensional quasi-periodic lattices[☆]

Claudia Comi[a,*], Marco Moscatelli[b], Jean-Jacques Marigo[b,c]

[a] Dept. Civil and Environmental Engineering Politecnico di Milano, Piazza L. da Vinci 32, Milan, 20133, Italy
[b] Institut Jean Le Rond d'Alembert Sorbonne Université and CNRS, UMR 7190, Paris, 75252, France
[c] Laboratoire de Mécanique des Solides Institut Polytechnique de Paris and CNRS, Palaiseau, 610101, France

ARTICLE INFO

Keywords:
Quasi-periodicity
Lattice
Band-gaps
Wave localization
Topological pumping

ABSTRACT

We study longitudinal wave propagation in a two-dimensional elastic lattice formed by parallel bars coupled by slender beams whose out-of-plane thickness is modulated according to an Aubry–André–Harper profile. This modulation can yield periodic or quasi-periodic architectures depending on the choice of the parameters. Starting from the continuous bar–beam model, we derive a discrete formulation and analyze the existence of bounded solutions and band-gaps as functions of the modulation amplitude and geometry. We provide analytical criteria for band-gap nucleation and explicit estimates of gap widths, and we show how quasi-periodicity can both create new gaps and shrink existing ones relative to the periodic case. The results offer new insights on the influence of quasi-periodicity in 2D elastic lattices. We show numerically how this class of structures can be exploited to achieve topological pumping of elastic waves.

1. Introduction

The propagation of elastic waves through periodic lattices has been extensively studied, starting from concepts originally put forward in the solid state physics by Brillouin (1953) and Kittel (1953). The topic has been, and still is, of rapidly growing interest, as it is central for the design of metamaterials in many applications, including vibration isolation (Palermo et al., 2016; De Ponti et al., 2020; Maurel et al., 2025), wave-guiding (Bonnecaze et al., 2003; Khelif et al., 2003; Faraci et al., 2023), and energy harvesting (Carrara et al., 2013; Lv et al., 2013). See also Jiao et al. (2023) for a recent review.

The results obtained for lattices have also been exploited to study the dynamics of periodic structures. Original significant contributions in this field are due to Miles (1956) and Mead (1970), who studied vibrations in beams laying on a periodic array of supports. Since then, there has been a substantial amount of work dedicated to the development of multifunctional metastructures. For instance, Madine and Colquitt (2022) dealt with the propagation of torsional–flexural waves in a square lattice of massless Euler–Bernoulli beams with the inertia being concentrated at the junctions, showing that such configuration can sustain negative refraction, mode trapping and beam splitting. In-plane axial–flexural waves were treated in Cabras et al. (2024) for a rectangular grid of Rayleigh beams, which are axially preloaded and endowed with sliding constraints, enabling for the presence of localization phenomena (see also Bordiga et al., 2022). Periodic framed beams were analyzed in Chesnais et al. (2015) and Rallu et al. (2018) by means of asymptotic techniques, to predict the presence of band-gaps generated by local resonances. More recently, experimental results have confirmed the waveguiding capacities of metastructures (Kannan et al., 2026).

The presence of frequency gaps in the spectra of metamaterials has been exploited to localize waves, and thus elastic energy, by introducing *defects* in the otherwise perfectly periodic structure, such as truncated boundaries, interfaces, or internal defects (Delourme et al., 2016; Rosa et al., 2023; Moscatelli et al., 2020; Davies and Craster, 2022). Nevertheless, reliance on perfect periodicity can represent a limitation in practical applications, where manufacturing imperfections and environmental factors can disrupt the idealized structure, possibly reducing the localization effect or, in the worst case, destroying it (Ammari et al., 2020). This has motivated the exploration of the robustness of wave localization phenomena.

In this sense, beyond purely periodic structures, quasi-periodic systems seem to offer additional design flexibility and reliability for controlling waves behavior. This new class of metamaterials is characterized by a Helmholtz governing equation whose operator is a quasi-periodic function of the spatial coordinates, and thus does not commute with translations.

In one-dimension, the most famous of such operators is the so-called *almost-Mathieu* operator (Asch et al., 2006; Harper, 1955), whose

[☆] This article is part of a Special issue entitled: 'Jean Lemaitre' published in European Journal of Mechanics / A Solids.

* Corresponding author.
E-mail address: claudia.comi@polimi.it (C. Comi).

https://doi.org/10.1016/j.euromechsol.2026.106194
Received 27 February 2026; Received in revised form 3 May 2026; Accepted 5 May 2026
Available online 9 May 2026

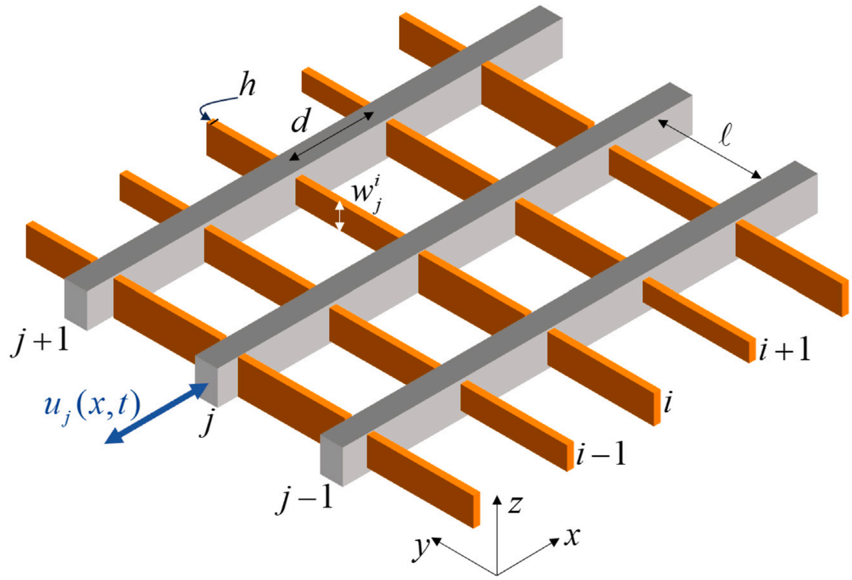

Fig. 1. Scheme of the considered system: two dimensional lattice with parallel bars (in gray, index j) and connecting beams (in orange, index i). (For interpretation of the references to color in this figure legend, the reader is referred to the web version of this article.)

associated Helmholtz equation, called *Harper equation*, is a discretization of the *Mathieu equation*. This model has been extensively studied for applications in condensed matter physics (Aubry and André, 1980; Hofstadter, 1976), and provides a mathematical framework for understanding wave localization and band-gap formation in this class of quasi-periodic systems.

For elastic waves, this model has been obtained through the so called *on-site* modulation (Martínez et al., 2018), e.g. by modulating in space the stiffness of resonators in locally resonant materials, both in one-dimensional (Martí-Sabaté and Torrent, 2021) and bi-dimensional configurations (Guo et al., 2024). Simultaneous space and time modulation have also been investigated (Pu et al., 2022), resulting in non-reciprocal wave propagation.

However, in mechanical metamaterials, quasi-periodicity was more often introduced through *off-site* modulation, by modulating either the stiffness or the spacing of the elements composing one-dimensional systems (Gei, 2010; Xia et al., 2020; LeGrande et al., 2024; Davies and Morini, 2024).

The extension of these concepts to two-dimensional mechanical systems is still less explored, although it holds great promise for advanced and robust wave manipulation capabilities, as demonstrated e.g. in acoustics (Ni et al., 2019), in optics (Kraus et al., 2012), and in mechanics (Rosa et al., 2019). This work points towards this direction. Specifically, we consider a two-dimensional metastructure consisting of parallel elastic bars aligned along the x-direction, periodically or quasi-periodically connected at discrete points by slender beams oriented along the y-direction (see Fig. 1). The out-of-plane thickness of these connecting beams is modulated in both x and y directions according to an Harper profile, creating either periodic arrangements (when the modulation parameters are rational) or genuinely quasi-periodic structures (when irrational). This geometric configuration extends previous results on periodic beam trusses (Marigo et al., 2023) to the quasi-periodic regime and builds upon recent works on quasi-periodic one-dimensional discrete systems (Comi et al., 2025; Moscatelli et al., 2024).

In this work, we perform a comprehensive analytical and numerical analysis of longitudinal wave propagation along the bars. First, we establish the exact solution to the dispersion relation that dictates the propagation of such waves in the network of bars and beams. Then, we characterize the band-gap structure for both periodic and quasi-periodic configurations, and identify how geometric parameters control wave propagation. The analysis combines continuous and discrete formulations, providing both theoretical insights and practical design guidance for engineered metamaterials. The results reveal that, contrary to the one-dimensional case, quasi-periodicity can induce or not new band-gaps and increase or reduce existing ones. We also illustrate the potential for topological pumping of elastic waves in these quasi-periodic lattices, demonstrating their promise for advanced wave manipulation applications.

The paper is organized as follows: Section 2 introduces the reference problem and derives the governing equations. In Section 2.1, an equivalent discrete formulation is derived, assuming the displacements at the nodes between bars and beams as unknowns. Section 2.2 presents the formulation, homogenized along the bars, for small beam spacing, while Section 2.3 addresses the discrete case when considering periodicity in one direction and quasi-periodicity in the other. In Section 3, focusing on the 2D periodic problem, we obtain complete, new analytic results on band-gaps appearance. The extension to quasi-periodic arrangements in performed in Section 4. Numerical results are provided in Section 5, and conclusions are drawn in Section 6.

2. Reference problem

Let us consider the two-dimensional linear elastic lattice schematically shown in Fig. 1, constituted by parallel bars along the x direction (in gray) connected, at discrete points $x = x^i$ located at fixed distance d, by slender beams of length ℓ, with axis in the y direction (in orange). For this system, we want to study the propagation of axial waves in the bars, labeled with the index j. In the linear regime this problem is decoupled from that related to flexural waves and hence can be treated separately.

The same elastic material, with Young modulus E and mass density ρ is assumed for both bars and beams to simplify the notation. The cross section of the bars is uniform and denoted by A, while the beams have uniform in plane thickness h, and possibly variable out of plane thickness w_j^i.

The two-dimensional periodicity can be considered as perfect or can be perturbed by modulating the out of plane thickness w_j^i of the beams both in the x and/or y directions. The Aubry–André–Harper profile (Aubry and André, 1980) is assumed in two dimensions

$$w_j^i = w_0\,[1 + R\cos(2\pi(\theta i + \phi j))]\,. \tag{1}$$

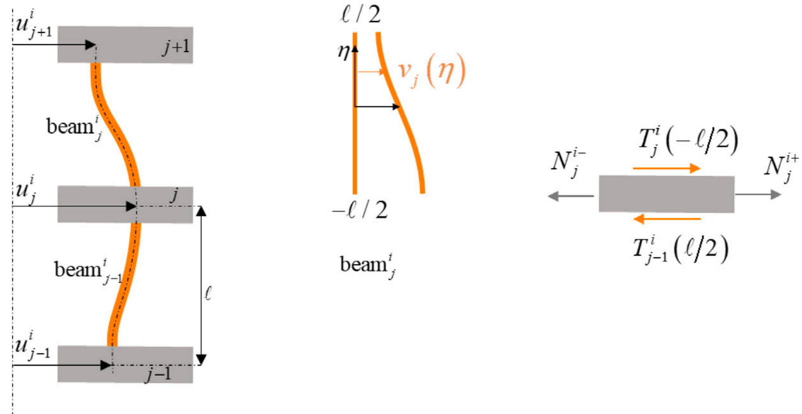

Fig. 2. Deformed configuration, local reference frame on beam^i_j and free-body diagram in bar j at $x = x^i$.

The rational and irrational θ and ϕ values define periodic and quasi-periodic patterns, respectively. For $\theta = 0$ and $\phi = 0$, all connecting beams are equal and the system is periodic of period d in x and period ℓ in y. We will refer to that case as 1-periodic case in x and y. For rational $\theta = \frac{p}{n}$ (p and n integers), the system has a periodicity of nd (is n-periodic) along x. Similarly, for rational $\phi = \frac{q}{m}$ (q and m integers), the system has a periodicity of $m\ell$ (is m-periodic) along y. Note that, when considering a lattice of finite dimensions, for n and m large enough, the system may not be large enough to contain one period of the infinite dimensional one.

For later use, we introduce three non-dimensional parameters characterizing the geometry of the considered system, namely the slenderness of the beams ϵ, the ratio between the bars and beams area α and the geometric anisotropy of the lattice δ

$$\epsilon = \frac{h}{\ell}, \quad \alpha = \frac{A}{hw_0}, \quad \delta = \frac{d}{\ell}. \tag{2}$$

The propagation of longitudinal waves of frequency ω along the bar j, at any $x \neq x^i$ is governed by the Helmholtz equation

$$\frac{\partial^2 u_j}{\partial x^2} + \Omega^2 u_j = 0, \tag{3}$$

where $\Omega = \omega\sqrt{\rho/E}$. At $x = x^i$ the axial force has a jump due to the shear forces T^i_{j-i} and T^i_j transmitted in $x = x^i$ by the two connection beams respectively below and above the considered bar j:

$$EA \left[\!\left[\frac{\partial u_j}{\partial x} \right]\!\right] (x_i) + T^i_j - T^i_{j-1} = 0. \tag{4}$$

The shear force T^i_{j-i} is given by the solution of the vibration problem of the beam located at $x = x^i$, subjected to imposed displacements $u_{j-1}(x^i) = u^i_{j-1}$ and $u_j(x^i) = u^i_j$ at its ends, while T^i_j corresponds to the beam located at $x = x^i$, subjected to imposed displacements u^i_j and u^i_{j+1} at its ends, see Fig. 2. The transversal vibration $v^i_j(\eta)$ of the slender beam j, located in $x = x_i$, for $-\frac{\ell}{2} \le \eta \le \frac{\ell}{2}$, is the solution of the following problem

$$\frac{h^2}{12}\frac{d^4 v^i_j}{d\eta^4} - \Omega^2 v^i_j = 0, \tag{5}$$

with the boundary conditions: $v^i_j(-\frac{\ell}{2}) = u^i_j$, $v^i_j(\frac{\ell}{2}) = u^i_{j+1}$, $\frac{dv^i_j}{d\eta}(\pm\frac{\ell}{2}) = 0$.

Defining the non-dimensional quantity[1]

$$\Lambda^4 = \frac{3\rho\omega^2}{4Eh^2}\ell^4 = \frac{3\Omega^2}{4h^2}\ell^4 = \frac{3}{4}\left(\frac{\Omega d}{\epsilon\delta}\right)^2, \tag{6}$$

the solution of (5) reads

$$v^i_j(\eta) = a_0 \cos 2\Lambda\frac{\eta}{\ell} + a_1 \sin 2\Lambda\frac{\eta}{\ell} + b_0 \cosh 2\Lambda\frac{\eta}{\ell} + b_1 \sinh 2\Lambda\frac{\eta}{\ell}, \tag{7}$$

with

$$\begin{aligned}
a_0 &= \frac{\sinh\Lambda}{\sinh\Lambda\cos\Lambda + \cosh\Lambda\sin\Lambda}\,\frac{u^i_j + u^i_{j+1}}{2},\\
a_1 &= \frac{-\cosh\Lambda}{\sinh\Lambda\cos\Lambda - \cosh\Lambda\sin\Lambda}\,\frac{u^i_{j+1} - u^i_j}{2},\\
b_0 &= \frac{\sin\Lambda}{\sinh\Lambda\cos\Lambda + \cosh\Lambda\sin\Lambda}\,\frac{u^i_j + u^i_{j+1}}{2},\\
b_1 &= \frac{\cos\Lambda}{\sinh\Lambda\cos\Lambda - \cosh\Lambda\sin\Lambda}\,\frac{u^i_{j+1} - u^i_j}{2}.
\end{aligned} \tag{8}$$

The shear force is then easily obtained by using $T^i_j = -\frac{Eh^3 w^i_j}{12}\frac{d^3 v^i_j}{d\eta^3}$. The net shear force transmitted to the bar at $x = x_i$ finally reads

$$\begin{aligned}
&T^i_j(-\frac{\ell}{2}) - T^i_{j-1}(\frac{\ell}{2}) = \\
&\left(\frac{2}{\ell}\right)^3 \frac{Eh^3}{12}\Big(w^i_j F(\Lambda)(u^i_{j+1} + u^i_j) + w^i_j G(\Lambda)(u^i_{j+1} - u^i_j) + \\
&\quad w^i_{j-1} F(\Lambda)(u^i_j + u^i_{j-1}) - w^i_{j-1} G(\Lambda)(u^i_j - u^i_{j-1})\Big),
\end{aligned} \tag{9}$$

where

$$F(\Lambda) = \Lambda^3 \frac{\tan(\Lambda)\tanh(\Lambda)}{\tan(\Lambda) + \tanh(\Lambda)}; \quad G(\Lambda) = \Lambda^3 \frac{1}{\tan(\Lambda) - \tanh(\Lambda)}. \tag{10}$$

Remark 1. Considering just two beams, say j and $j+1$, the contribution in (9) proportional to the sum $u^i_{j+1} + u^i_j$ corresponds to a symmetric solution, as considered in Comi et al. (2025), while that proportional to the difference $u^i_{j+1} - u^i_j$ corresponds to an antisymmetric one.

2.1. The general discrete formulation

The jump condition on the axial stress in the bar j at the points i where the beams are attached reads (see Fig. 2, right)

$$\begin{aligned}
&A\left[\!\left[\frac{\partial u_j}{\partial x}\right]\!\right](x_i) + \frac{2}{3}\left(\frac{h}{\ell}\right)^3 \Big(F(\Lambda)(w^i_j(u^i_{j+1} + u^i_j) + w^i_{j-1}(u^i_j + u^i_{j-1})) + \\
&\quad G(\Lambda)(w^i_j(u^i_{j+1} - u^i_j) + w^i_{j-1}(u^i_{j-1} - u^i_j))\Big) = 0 \quad \forall i \in \mathbb{N}.
\end{aligned} \tag{11}$$

Eq. (3) can be integrated along the bar j in each interval between the beams; the solution in $(x^{i-1} - x^i)$ and $(x^i - x^{i+1})$ reads, respectively

$$u_j(x) = u^i_j \cos\Omega(x - x^i) + \frac{-u^{i-1}_j + u^i_j \cos\Omega d}{\sin\Omega d}\sin\Omega(x - x^i), \tag{12}$$

[1] We will often refer to Λ as the "dimensionless frequency", or just "frequency".

$$u_j(x) = u_j^i \cos \Omega(x - x^i) + \frac{u_j^{i+1} - u_j^i \cos \Omega d}{\sin \Omega d} \sin \Omega(x - x^i). \tag{13}$$

The jump of its derivative in $x = x^i$ is hence

$$\left[\!\left[\frac{\partial u_j}{\partial x} \right]\!\right](x_i) = \frac{\Omega}{\sin \Omega d}(u_j^{i+1} + u_j^{i-1} - 2u_j^i \cos \Omega d). \tag{14}$$

Combining Eqs. (11) and (14) one finally obtains the discrete problem, holding at each node i, j of the lattice, point of intersection between bars and beams

$$\begin{aligned} &\frac{\Omega}{\sin \Omega d}(u_j^{i+1} + u_j^{i-1} - 2u_j^i \cos \Omega d) + \\ &\quad \frac{2}{3A}\left(\frac{h}{\ell}\right)^3 \Big(F(\Lambda)(w_j^i(u_{j+1}^i + u_j^i) + w_{j-1}^i(u_j^i + u_{j-1}^i)) + \\ &\quad G(\Lambda)(w_j^i(u_{j+1}^i - u_j^i) - w_{j-1}^i(u_j^i - u_{j-1}^i)) \Big) = 0 \quad \forall i, j \in \mathbb{N}. \end{aligned} \tag{15}$$

From now on, to simplify the subsequent developments, we will assume that $\Omega d \ll 1$. Eq. (15) hence simplifies to

$$\begin{aligned} &\left(u_j^{i+1} + u_j^{i-1} - 2u_j^i \left(1 - \frac{(\Omega d)^2}{2}\right) \right) + \\ &\quad \frac{2d}{3A}\left(\frac{h}{\ell}\right)^3 \Big(F(\Lambda)(w_j^i(u_{j+1}^i + u_j^i) + w_{j-1}^i(u_j^i + u_{j-1}^i)) + \\ &\quad G(\Lambda)(w_j^i(u_{j+1}^i - u_j^i) - w_{j-1}^i(u_j^i - u_{j-1}^i)) \Big) = 0 \quad \forall i, j \in \mathbb{N}. \end{aligned} \tag{16}$$

2.2. Homogenized formulation in x direction

When, in addition to the hypothesis $\Omega d \ll 1$, the distance between the connecting beams tends to zero, or when studying the propagation of waves with wavelength by far greater than d, we can consider a continuous distribution of connecting elements between the bars with a continuous variation of the out of plane thickness in the x direction as in Fig. 3. In this case the index i is replaced by x/d, and the out of plane thickness reads $w_j(x) = w_0 \left[1 + R\cos(2\pi(\theta x/d + \phi j))\right]$. We can interpret $2\pi\theta x/d$ as a phase, linearly varying along the bars, while the periodicity or quasi-periodicity in y is defined by rational or irrational values of ϕ. The distributed shear force transmitted to the bars $t_j(x)$ is related to the shear force T_j^i previously computed by $t_j(x_i) = T_j^i/d$.

In such case, Eq. (16) can be approximated by the following (scalar) differential equation :

$$\begin{aligned} &\frac{d^2u_j(x)}{dx^2} + \Omega^2 u_j(x) \\ &\quad + \frac{2h^3}{3A\ell^3 d}\Big(F(\Lambda)(w_j(x)(u_{j+1}(x) + u_j(x)) + w_{j-1}(x)(u_j(x) + u_{j-1}(x))) \\ &\quad + G(\Lambda)(w_j(x)(u_{j+1}(x) - u_j(x)) + w_{j-1}(x)(u_{j-1}(x) - u_j(x))) \Big) = 0, \end{aligned} \tag{17}$$

where $u_j(x)$ is now a continuous function of the position x along the bars. By rearranging (17) we obtain:

$$\begin{aligned} &\frac{d^2u_j(x)}{dx^2} + u_j(x)\left(\Omega^2 + \frac{2h^3}{3A\ell^3 d}(F(\Lambda) - G(\Lambda))(w_j(x) + w_{j-1}(x)) \right) \\ &\quad + \frac{2h^3}{3A\ell^3 d}\Big((F(\Lambda) + G(\Lambda))\big(w_j(x)u_{j+1}(x) + w_{j-1}(x)u_{j-1}(x)\big) \Big) = 0. \end{aligned} \tag{18}$$

If we make the hypothesis that not only Ωd, but also Λ is small, the functions $F(\Lambda)$ and $G(\Lambda)$ defined in Eq. (10) can be approximated as:

$$F(\Lambda) \approx \Lambda^4/2, \quad G(\Lambda) \approx 3/2. \tag{19}$$

Accordingly, the term $F(\Lambda) + G(\Lambda)$ in Eq. (18) can be approximated by $3/2$. The term $F(\Lambda) - G(\Lambda)$ cannot be approximated in the same way, as $\Omega^2 = \mathcal{O}(\Lambda^4)$. We thus have to consider the following term from Eq. (18):

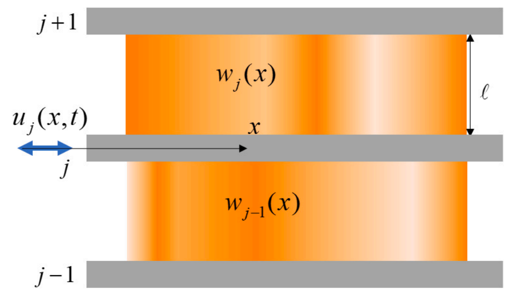

Fig. 3. Homogenized system in x direction for small d.

$$\Omega^2 + \frac{2h^3}{3A\ell^3 d}F(\Lambda)(w_j(x) + w_{j-1}(x)) \approx \Omega^2\left(1 + \frac{1}{4}\frac{1}{\alpha\delta}\frac{w_j(x) + w_{j-1}(x)}{\omega_0}\right). \tag{20}$$

If we also assume that the area of the bars A is greater with respect to the mean area of the connecting beams (i.e. $\alpha \gg 1$, from relation (2)) we can replace the term (20) by Ω^2, thus obtaining

$$\begin{aligned} &\frac{d^2u_j(x)}{dx^2} + \Omega^2 u_j(x) - \frac{\epsilon^3}{Ad}\ \big(u_j(x)(w_j(x) + w_{j-1}(x)) \\ &\quad - u_{j+1}(x)w_j(x) - u_{j-1}(x)w_{j-1}(x) \big) = 0. \end{aligned} \tag{21}$$

The above equation will be numerically solved in Section 5 to show the appearance of adiabatic pumping waves in the considered quasi-periodic system.

Remark 2. If the thickness $w_j(x)$ is the same for all the j, i.e. $w_j(x) = w(x) = w_0[1 + R\cos\frac{2\pi\theta}{d}x]$, by studying a solution of the form $u(x) = U(x)e^{\mathrm{i}\kappa j}$ Eq. (17) becomes:

$$\frac{d^2U(x)}{dx^2} + \left(\Omega^2 + \frac{8h^3}{3A\ell^3 d}w(x)\left(F(\Lambda)\cos^2\frac{\kappa}{2} - G(\Lambda)\sin^2\frac{\kappa}{2} \right) \right) U(x) = 0$$

which is a Mathieu equation, see e.g. Brillouin (1953).

2.3. The discrete problem, periodic in y and quasi-periodic in x

We now consider again the discrete formulation of Section 2.1 and we specialize it to the case where the out of plane thickness depends on i only, namely

$$w_j^i = w^i = w_0\left[1 + R\cos(2\pi\theta i)\right]. \tag{22}$$

Eq. (16) can then be rewritten as

$$\begin{aligned} &\Delta^i u_j^{\bullet} + (\Omega d)^2 u_j^i + \\ &\quad \frac{2w^i d}{3A}\left(\frac{h}{\ell}\right)^3 \left((F(\Lambda) + G(\Lambda))\Delta_j u_{\bullet}^i + 4F(\Lambda)u_j^i \right) = 0 \quad \forall i, j \in \mathbb{N} \end{aligned} \tag{23}$$

where we introduced the discrete Laplacian operators in the x and y directions

$$\Delta^i u_j^{\bullet} = u_j^{i+1} + u_j^{i-1} - 2u_j^i, \quad \Delta_j u_{\bullet}^i = u_{j+1}^i + u_{j-1}^i - 2u_j^i. \tag{24}$$

Let us consider displacements which are periodic in the y-direction, that is, u_j^i under the following form

$$u_j^i = U^i \exp(\mathrm{i}\,\kappa j), \tag{25}$$

where $\kappa = k_y\ell$, k_y denoting the given wave number in the direction y. The values $\kappa = \beta 2\pi$, $\beta \in \mathbb{Z}$, correspond to the case where the two ends of each bent beam move in phase (symmetric solution of (7)), while

$\kappa = \pi + \beta 2\pi$, $\beta \in \mathbb{Z}$, correspond to the case where their motion is in opposition of phase (skew-symmetric solution of (7)). From (25), one gets that the displacements $\{U^i\}_{i\in\mathbb{N}}$ must satisfy the following discrete equation: $\forall i \in \mathbb{N}$,

$$\Delta^i U^\bullet + \lambda_0 \left(\frac{\mu_0}{2}\Lambda^4 + \big(1 + R\cos(2i\theta\pi)\big)\Big(F(\Lambda)\cos^2\frac{\kappa}{2} - G(\Lambda)\sin^2\frac{\kappa}{2}\Big)\right) U^i = 0, \tag{26}$$

where λ_0 and μ_0 are the two dimensionless parameters defined by

$$\lambda_0 = \frac{8h^3 d w_0}{3A\ell^3}, \qquad \mu_0 = \frac{Ad}{h\ell w_0}. \tag{27}$$

For the interpretation of the results, it is useful to express λ_0 and μ_0 in terms of the dimensionless parameters previously introduced (relations (2))

$$\lambda_0 = \frac{8}{3}\frac{\delta}{\alpha}\epsilon^2, \qquad \mu_0 = \delta\alpha. \tag{28}$$

Remark 3. Since the parameter ϵ characterizing the slenderness of beams must be small for the classical theory of beams to be applicable, the parameter λ_0 must also be small as soon as δ/α is of the order of 1 or smaller. Moreover, the condition $\Omega d \ll 1$ requires that $\Lambda \ll \sqrt{1/(\epsilon\delta)}$. Consequently, in the applications developed below we will only consider small values of the parameter λ_0 and dimensionless frequencies Λ not too large.

Remark 4. If we consider the case where the bars and the beams have the same width h and the bars have thickness w_0, then $\alpha = 1$ and the two parameters in (27) simply become $\mu_0 = \delta$ and $\lambda_0 = \frac{8}{3}\epsilon^2\mu_0$.

3. Periodic case

3.1. Setting of the problem

When $R = 0$ or $\theta \in \{0, 1\}$, the two-dimensional system of stretched bars and bent beams is periodic; the in-plane periodic cell corresponds to a rectangle of size d in the x-direction and of size ℓ in the y-direction (if one neglects the in-plane thickness of the bars and of the beams with respect to their distance). The parameter μ_0 represents the ratio between the mass of the part of the stretched bars over the mass of the bent beams included in the periodic cell, whereas λ_0 is a coefficient denoting the anisotropy of the effective elastic stiffness between the directions x and y. In that case, the discrete equation governing the displacements of the periodic system can be read as

$$\Delta^i U^\bullet + \lambda U^i = 0, \qquad \forall i \in \mathbb{N}, \tag{29}$$

with

$$\lambda = \hat\lambda(\kappa, \Lambda) := \lambda_0 \left(\frac{\mu_0}{2}\Lambda^4 + F(\Lambda)\cos^2\frac{\kappa}{2} - G(\Lambda)\sin^2\frac{\kappa}{2}\right). \tag{30}$$

3.2. The dispersion equation of harmonic plane waves

The general solution of (29) is well known and has been studied in Comi et al. (2025), Moscatelli et al. (2024). Let us recall here the main results.

1. If $0 < \lambda < 4$, then, setting $\lambda = 2(1 - \cos k) = 4\sin^2\frac{k}{2}$ with $k \in (0, +\pi)$, the general solution of (29) is of the form $U^i = U_0\cos(ki) + V_0\sin(ki)$ for $i \in \mathbb{N}$ where U_0 and V_0 are two arbitrary constants.
2. If $\lambda < 0$ or $\lambda > 4$, then, setting $\lambda = 2(1 \pm \cosh k)$ with $k > 0$, the general solution of (29) is of the form $U^i = U_0\cosh(ki) + V_0\sinh(ki)$ when $\lambda < 0$ and of the form $U^i = U_0(-1)^i\cosh(ki) + V_0(-1)^i\sinh(ki)$ when $\lambda > 4$, where U_0 and V_0 are two arbitrary constants.
3. If $\lambda = 0$, then the general solution of (29) reads as $U^i = U_0 + iV_0$, whereas, if $\lambda = 4$, then the general solution of (29) reads as $U^i = (-1)^i\big(U_0 + iV_0\big)$.

Accordingly, when $0 \le \lambda \le 4$, the displacements u^i_j of the nodes of the system of bars and beams reads as $u^i_j = U\exp[\mathrm{i}(ki + \kappa j)]$ which corresponds to a motion of an harmonic plane wave whose wave vector components are (k_x, k_y), with $k = k_x d$. From definition (30) of λ, one obtains the following dispersion equation giving the relation between the normalized wave vector (k, κ) and the dimensionless frequency Λ:

$$4\sin^2\frac{k}{2} = \lambda_0\left(\frac{\mu_0}{2}\Lambda^4 + F(\Lambda)\cos^2\frac{\kappa}{2} - G(\Lambda)\sin^2\frac{\kappa}{2}\right). \tag{31}$$

When $\lambda \notin [0, 4]$, such harmonic waves cannot propagate in the system of bars and beams.

Introducing, as in Marigo et al. (2023), the effective masses $m_a(\Lambda)$ and $m_s(\Lambda)$:

$$m_a(\Lambda) = \mu_a(\Lambda)m_{\mathrm{f}}, \quad m_s(\Lambda) = \mu_s(\Lambda)m_{\mathrm{f}} \tag{32}$$

with

$$m_{\mathrm{f}} = \rho h\ell w_0, \quad \mu_a(\Lambda) = \mu_0 - \frac{2G(\Lambda)}{\Lambda^4} \quad \text{and} \quad \mu_s(\Lambda) = \mu_0 + \frac{2F(\Lambda)}{\Lambda^4}, \tag{33}$$

the dispersion relation (31) becomes

$$4\sin^2\frac{k}{2} = \frac{\lambda_0}{2}\Lambda^4\left(\mu_s(\Lambda)\cos^2\frac{\kappa}{2} + \mu_a(\Lambda)\sin^2\frac{\kappa}{2}\right). \tag{34}$$

The mass $m_a(\Lambda)$ represents the effective mass of the periodic cell when the two ends of each bent beam vibrate in opposition of phase at the dimensionless frequency Λ, while the mass $m_s(\Lambda)$ represents the effective mass when the ends of the beams vibrate in phase. The dispersion relation (34) is similar to that studied in Marigo et al. (2023) (see equation (3)). It differs simply by the fact that the term $4\sin^2 k/2$ in (34) is replaced by k^2 in Marigo et al. (2023) where only the case of small k was considered.

The study of the dispersion Eq. (31) can be made with the wave vector (k_x, k_y) varying only in the first Irreducible Brillouin Zone (IBZ) $[0, \frac{\pi}{d}] \times [0, \frac{\pi}{\ell}]$, by symmetry. Note that, being the unit cell rectangular, also the reciprocal lattice has rectangular, non-isotropic, cells. However, to simplify the notation, we consider again the non-dimensional wave numbers (k, κ), hence, the corresponding IBZ becomes the square $[0, \pi]^2$, see Fig. 4.

3.3. Some properties of the dispersion equation

Let us denote by Λ^s_I and Λ^a_I the ordered sequences of frequencies of resonance of the bent beams:

$$0 < \cdots < \Lambda^s_I < \Lambda^a_I < \Lambda^s_{I+1} < \Lambda^a_{I+1} < \cdots, \qquad I \in \mathbb{N}^*$$

where Λ^s_I is the unique solution of the equation $\tan\Lambda + \tanh\Lambda = 0$ with $\Lambda \in (I\pi - \pi/2, I\pi)$ and Λ^a_I is the unique solution of the equation $\tan\Lambda - \tanh\Lambda = 0$ with $\Lambda \in (I\pi, I\pi + \pi/2)$. The frequencies Λ^s_I are associated to symmetric modes of resonance whereas the Λ^a_I's are associated with skew-symmetric modes. Moreover we set $\Lambda^a_0 = 0$. Since $\tanh\Lambda$ is rapidly equal to 1 when Λ grows, good approximations of those frequencies are

$$\Lambda^s_I \approx I\pi - \pi/4, \qquad \Lambda^a_I \approx I\pi + \pi/4 \qquad \text{for } I > 1. \tag{35}$$

The properties of the dispersion Eq. (31) are essentially due to the following properties of the functions F and G, see Fig. 5:

1. The function F increases continuously from 0 to $+\infty$ in the interval $[0, \Lambda^s_1)$ and from $-\infty$ to $+\infty$ in each interval $(\Lambda^s_I, \Lambda^s_{I+1})$ for $i \in \mathbb{N}^*$;
2. The function G decreases continuously from $3/2$ to $-\infty$ in the interval $[0, \Lambda^a_1)$ and from $+\infty$ to $-\infty$ in each interval $(\Lambda^a_I, \Lambda^a_{I+1})$ for $i \in \mathbb{N}^*$;
3. The function $F + G$ is positive in each interval $(\Lambda^a_{I-1}, \Lambda^s_I)$ and negative in each interval $(\Lambda^s_I, \Lambda^a_I)$ for $i \in \mathbb{N}^*$.

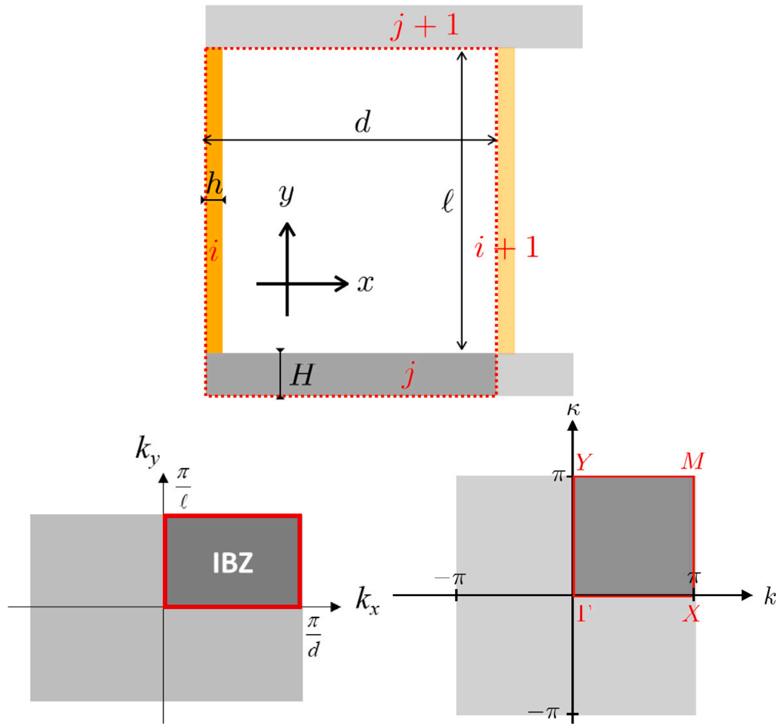

Fig. 4. In-plane periodic cell of the system of bars and beams and First Brillouin Zone, with the IBZ highlighted in dark gray, of the wave vector (k_x, k_y) (left) and of the normalized wave vector (k, κ) (right).

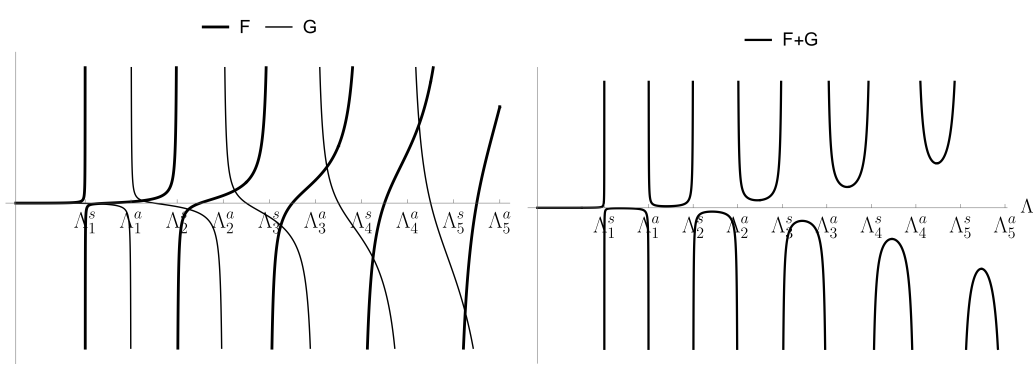

Fig. 5. Graphs of the functions F and G (left), and of $F+G$ (right).

3.3.1. Location of the pass-bands and band-gaps

The goal of this section is to determine the frequencies at which plane harmonic waves can propagate in the system of bars and beams. Such a frequency, characterized by its associated dimensionless value Λ, is then a value of $\Lambda \in [0, +\infty)$ for which there exists a real wave vector $(k, \kappa) \in [0, \pi]^2$ satisfying the dispersion Eq. (31). Recalling the definition (30) of function $\hat{\lambda}(\kappa, \Lambda)$, defined in $[0, \pi] \times [0, +\infty)$, this is equivalent to find the Λ's such that $\hat{\lambda}(\kappa, \Lambda) \in [0, 4]$ for some $\kappa \in [0, \pi]$. An interval of frequencies made of such Λ is said a pass-band while an interval of frequencies made of Λ for which there exists no wave vector satisfying the dispersion equation is called a band-gap. (Those intervals can be open, semi-open or closed.) Let us remark that $\Lambda = 0$ belongs to a pass-band because $\hat{\lambda}(0, 0) = 0$.

By virtue of the properties of the functions F and G described in Section 3.3, we obtain the following proposition, the proof of which is given in the Appendix A, concerning the location of the pass-bands and the band-gaps:

Proposition 1. *Considering separately each interval* $[0, \Lambda_1^s]$ *and* $(\Lambda_I^s, \Lambda_I^a]$, $(\Lambda_I^a, \Lambda_{I+1}^s]$ *for* $I \in \mathbb{N}^*$, *one has*

- *If* $\hat{\lambda}(\pi, \Lambda_1^s) \le 4$, *then* $[0, \Lambda_1^s]$ *is a pass-band; else, then* $[0, \Lambda_0]$ *is a pass-band while* $(\Lambda_0, \Lambda_1^s]$ *is a band-gap, where* Λ_0 *is the unique solution of* $\hat{\lambda}(\pi, \Lambda) = 4$ *with* $\Lambda \in (0, \Lambda_1^s)$;
- *If* $\hat{\lambda}(0, \Lambda_I^a) \le 4$, *then* $(\Lambda_I^s, \Lambda_I^a]$ *is a pass-band; else, then* $(\Lambda_I^s, \Lambda_{2I+1}]$ *is a pass-band while* $(\Lambda_{2I+1}, \Lambda_I^a]$ *is a band-gap, where* Λ_{2I+1} *is the unique solution of* $\hat{\lambda}(0, \Lambda) = 4$ *with* $\Lambda \in (\Lambda_I^s, \Lambda_I^a)$;
- *If* $\hat{\lambda}(\pi, \Lambda_{I+1}^s) \le 4$, *then* $(\Lambda_I^a, \Lambda_{I+1}^s]$ *is a pass-band; else, then* $(\Lambda_I^a, \Lambda_{2I}]$ *is a pass-band while* $(\Lambda_{2I}, \Lambda_{I+1}^s]$ *is a band-gap, where* Λ_{2I} *is the unique solution of* $\hat{\lambda}(\pi, \Lambda) = 4$ *with* $\Lambda \in (\Lambda_I^a, \Lambda_{I+1}^s)$.

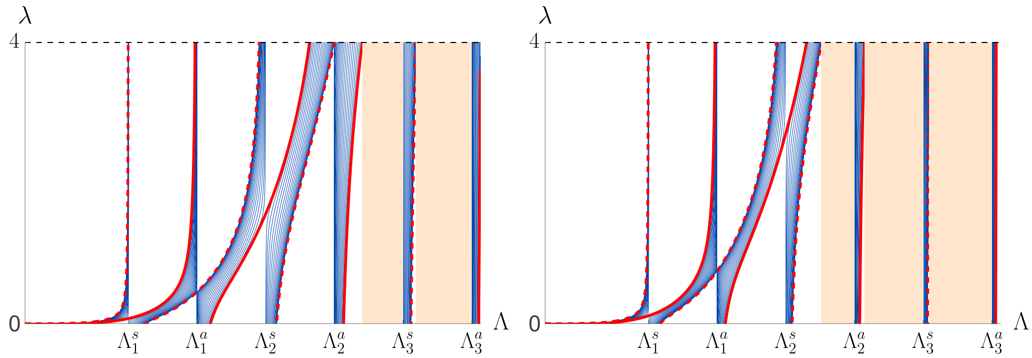

Fig. 6. Family of curves $\hat{\lambda}$ versus dimensionless frequency Λ: blue curves correspond to $\kappa \in (0,\pi)$, dashed red curves correspond to $\kappa = 0$ (side ΓX of the first Brillouin zone), solid bold red curves correspond to $\kappa = \pi$ (side YM of the first Brillouin zone) for $\lambda_0 = 0.005$ and $\mu_0 = 0.5$ (left) or $\mu_0 = 1$ (right); band-gaps are shaded in light orange. (For interpretation of the references to color in this figure legend, the reader is referred to the web version of this article.)

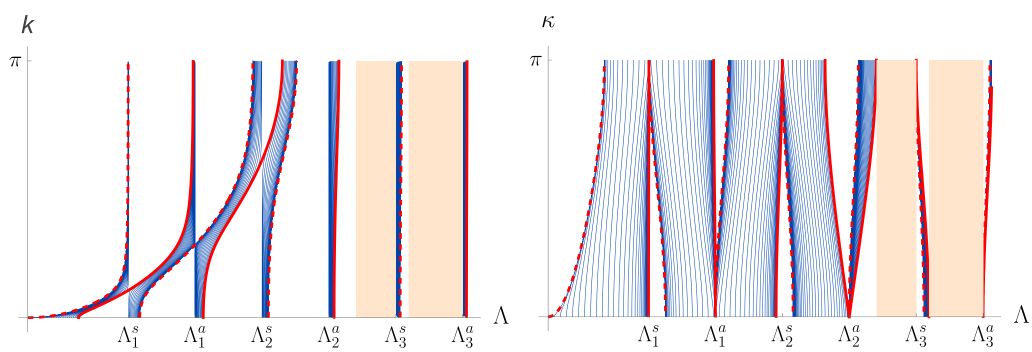

Fig. 7. Left: family of curves k versus dimensionless frequency Λ: blue curves correspond to $\kappa \in (0,\pi)$, dashed red curves correspond to $\kappa = 0$ (side ΓX of the first Brillouin zone), solid bold red curves correspond to $\kappa = \pi$ (side YM of the first Brillouin zone). Right: family of curves κ versus dimensionless frequency Λ: blue curves correspond to $k \in (0,\pi)$, dashed red curves correspond to $k = 0$ (side ΓY of the first Brillouin zone), solid bold red curves correspond to $\kappa = \pi$ (side XM of the first Brillouin zone). $\lambda_0 = 0.005$ and $\mu_0 = 0.5$, band-gaps shaded in light orange. (For interpretation of the references to color in this figure legend, the reader is referred to the web version of this article.)

Therefore, it suffices to compare $\hat{\lambda}(\pi, \Lambda_I^s)$ and $\hat{\lambda}(0, \Lambda_I^a)$ to 4 to determine whether a band-gap exists in a given interval. By virtue of (10) and the definitions of Λ_I^s and Λ_I^a, one has

$$\hat{\lambda}(\pi, \Lambda_I^s) = \frac{\lambda_0}{2} {\Lambda_I^s}^3 \left(\mu_0 \Lambda_I^s + \coth \Lambda_I^s\right), \quad \hat{\lambda}(0, \Lambda_I^a) = \frac{\lambda_0}{2} {\Lambda_I^a}^3 \left(\mu_0 \Lambda_I^a + \tanh \Lambda_I^a\right),$$

and hence, by virtue of (35), one gets

$$\hat{\lambda}(\pi, \Lambda_I^s) < \hat{\lambda}(0, \Lambda_I^a) < \hat{\lambda}(\pi, \Lambda_{I+1}^s)\ \forall i \geq 1 \quad \text{and} \quad \lim_{i\to\infty} \hat{\lambda}(\pi, \Lambda_I^s) = +\infty.$$

Consequently, one has the following remarkable result:

Proposition 2. *Band-gap exists in the interval $(\Lambda_I^s, \Lambda_I^a]$ or $(\Lambda_I^a, \Lambda_{I+1}^s]$ for I large enough, and, as soon as a band-gap exists in an interval, all the subsequent intervals contain a band-gap.*

3.3.2. Dependence on λ_0 and μ_0

For a given μ_0, if λ_0 is large enough so that $\hat{\lambda}(\pi, \Lambda_1^s) > 4$, then each interval between subsequent symmetric and non-symmetric eigenfrequencies contains a band-gap. Otherwise, the first intervals are pass-bands. When $\lambda_0 \ll 1$ (which is the usual situation), the first index i at which a band-gap exists is of the order of $\lambda_0^{-1/4}$ when μ_0 is of the order of 1, and of the order of $\lambda_0^{-1/3}$ when $\mu_0 \ll 1$.

For a given λ_0, the first index i at which a band-gap exists is a decreasing function of μ_0.

Fig. 6 shows an example of the above results for $\lambda_0 = 0.005$. The family of blue curves represents $\hat{\lambda}(\kappa, \Lambda)$ defined in Eq. (30) for fixed κ, ranging from 0 to π, the dashed red curve corresponds to $\kappa = 0$ (side ΓX of the first Brillouin zone), the solid red curve corresponds to $\kappa = \pi$ (side YM of the first Brillouin zone), the intervals of frequency such that no curves exist in the range $0 \leq \hat{\lambda} \leq 4$ are the band-gaps (shaded in light orange). The left and right plot correspond to $\mu_0 = 0.5$ and $\mu_0 = 1$, respectively: as expected the first band-gap appears at lower frequency as μ_0 increases.

The same results can be obtained by representing the solution of Eq. (31) in terms of one of the wave number (k or κ) versus the non-dimensional frequency Λ when the other wave number (κ or k) runs from 0 to π. Again the set of curves cover only part of the frequency axis; the intervals which are not reached correspond to band-gaps. Fig. 7 shows the result for the same parameters used in Fig. 6 left: the same band gaps are found.

3.3.3. Dependence of band-gaps on geometric parameters

Even though the dispersion properties only depend on two non-dimensional parameters λ_0 and μ_0, more physical insight can be obtained by considering separately the dependence on the slenderness ϵ, on the beam-bar area ratio α and on the geometric anisotropy ratio δ. The results are summarized in Fig. 8.

The effect of different geometric anisotropy, i.e., different δ, can be seen by comparing Figs. 8a and 8b. For fixed slenderness and ratio of areas, by decreasing δ, i.e., when the distance between the beams decreases with respect to the length of the beams, the first band-gap shifts to higher frequencies.

The ratio α between the area of the bars and the beams has an influence on the width of the band. Namely, for fixed ϵ and δ, when α increases, the band-gap width increases (cf. Figs. 8a and 8c).

Finally, when the slenderness of the beams decreases, i.e. when ϵ increases, the first band-gap shifts to lower frequency (cf. Figs. 8a and 8d); note, however, that the relation between Λ and the actual

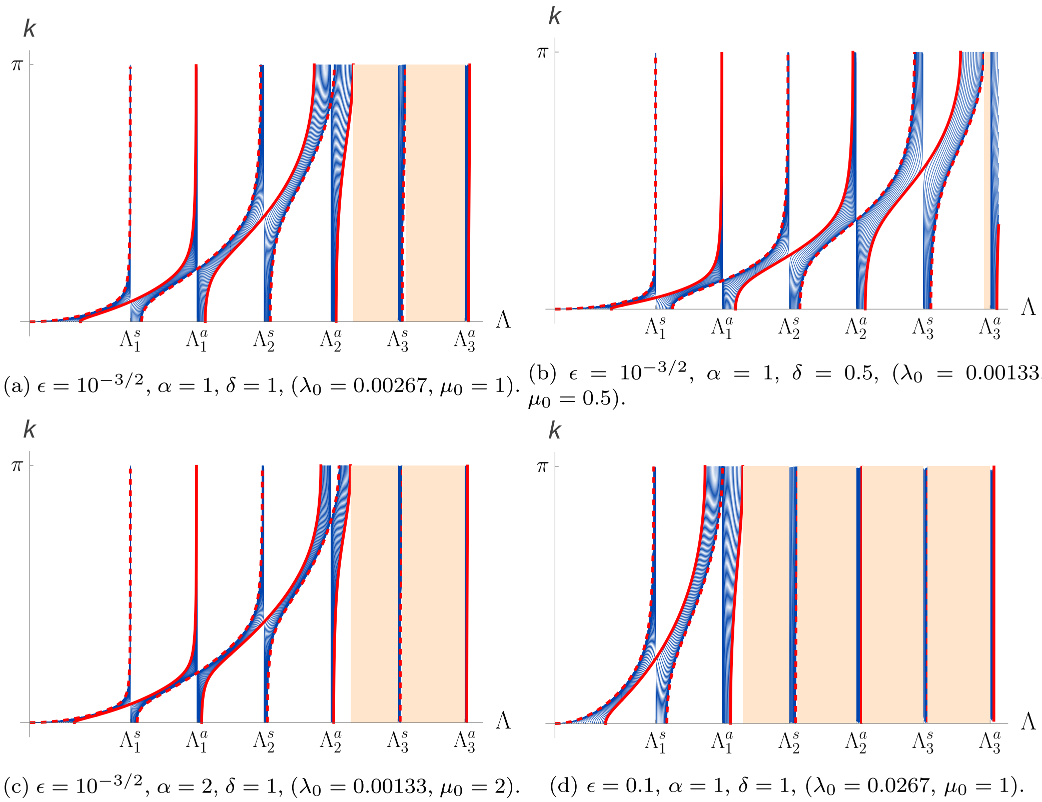

(a) $\epsilon = 10^{-3/2}$, $\alpha = 1$, $\delta = 1$, ($\lambda_0 = 0.00267$, $\mu_0 = 1$).

(b) $\epsilon = 10^{-3/2}$, $\alpha = 1$, $\delta = 0.5$, ($\lambda_0 = 0.00133$, $\mu_0 = 0.5$).

(c) $\epsilon = 10^{-3/2}$, $\alpha = 2$, $\delta = 1$, ($\lambda_0 = 0.00133$, $\mu_0 = 2$).

(d) $\epsilon = 0.1$, $\alpha = 1$, $\delta = 1$, ($\lambda_0 = 0.0267$, $\mu_0 = 1$).

Fig. 8. Band-gaps at varying ϵ, α and δ (meaning of the curves as in Fig. 7 left).

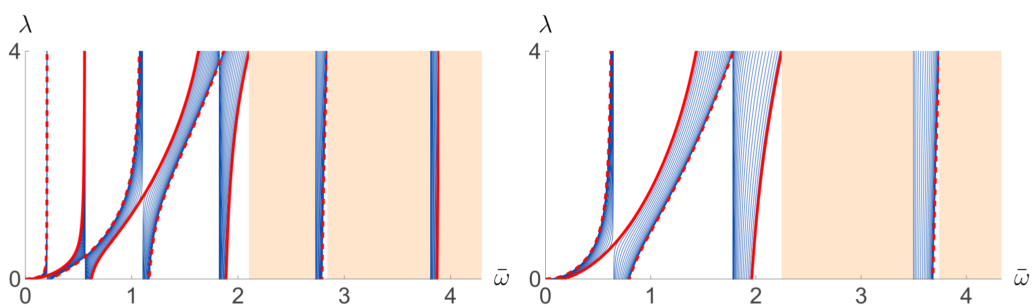

Fig. 9. $\epsilon = 10^{-3/2}$ ($\lambda_0 = 0.0027$ and $\mu_0 = 1$), $\epsilon = 0.1$, ($\lambda_0 = 0.027$ and $\mu_0 = 1$).

frequency ω also depends on ϵ. When the band-gaps are represented in terms of the actual nondimensional frequency $\bar{\omega} = \omega\ell/c$, $c = \sqrt{E/\rho}$ being the material celerity, one can observe that, if only the slenderness ϵ changes, the first band-gap opens at a similar frequency, see Fig. 9.

4. Analysis of the discrete problem with quasi-periodicity in x

We now consider the discrete problem defined by Eq. (26) where $\kappa \in [0, \pi]$ is the wave number in the direction y, $\theta \in (0, 1)$ is the quasi-periodicity parameter and $R \in [-1, +1]$ is a parameter measuring the "gap" to the periodicity of the out-of-plane thickness. In order to follow the method developed in Moscatelli et al. (2024), Comi et al. (2025), we formulate the discrete Eq. (26) as follows:

$$\forall i \in \mathbb{N},\ \Delta^i U^\bullet + \lambda(1 + R_* \cos 2i\theta\pi)U^i = 0 \tag{36}$$

with

$$R_* = \left(1 - \frac{\mu_0 \Lambda^4}{2\lambda}\right) R. \tag{37}$$

Let us first remark that it suffices to consider $\theta \in (0, 1/2]$ because the problem is unchanged when θ is changed into $1 - \theta$. The question is to determine, for a given θ, at which conditions on the data entering in the definition of λ and R_*, the system (36)–(37) admits non trivial bounded solutions $\{U^i\}_{i\in\mathbb{N}}$. For that, we will essentially follow the method presented in Moscatelli et al. (2024), Comi et al. (2025) that we briefly recall here.

We set

$$d_i = 1 + R_* \cos 2i\theta\pi.$$

However, here R_* will depend in general on κ and Λ, and is not a constant equal to R except when $\mu_0 \ll 1$. Therefore, even if one has only to consider the case where $|R| < 1$ (so that the thickness of the beams remains always positive), R_* can take any real value. As far as the parameter θ is concerned, we first consider rational values for θ, namely $\theta = p/n$ with p and n integers such that $0 < p \leq n/2$. Thus the system is periodic of period n. Introducing $\bar{U}^i = U^{ni}$ for $i \in \mathbb{N}$, the sequence of the $\bar{U}^i$'s is solution of the following discrete system:

$$\Delta^i \bar{U}^\bullet + \mu \bar{U}^i = 0, \quad \forall i \in \mathbb{N}$$

where μ is a polynomial of degree n in λ whose coefficients depend on p, n and R_*, see Moscatelli et al. (2024), Comi et al. (2025) for the

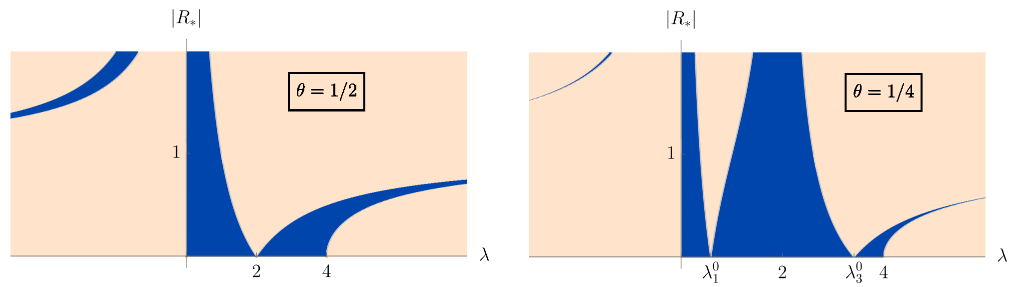

Fig. 10. In blue, evolution with R_* of the domain of admissibility of λ for the existence of periodic solutions in the cases where $\theta = 1/2$ (left) or $\theta = 1/4$ (right). (For interpretation of the references to color in this figure legend, the reader is referred to the web version of this article.)

details. That system admits bounded (and in fact periodic) solutions if and only if $\mu \in [0,4]$. Therefore, denoting by $\mu_n^{R_*}(\lambda)$ the polynomial giving μ, the system (36) admits itself bounded (and in fact n-periodic) solutions if and only if λ is such that $\mu_n^{R_*}(\lambda) \in [0,4]$.

However, a complete analysis is only possible for small values of n because the explicit construction of the polynomial then becomes treatable; when n is large (and when θ is irrational) the analysis can be performed only for small values of R. Therefore, we first fully treat the cases $n = 2$ and $n = 4$ before presenting partial results for the general case.

4.1. Cases where $n = 2$ or 4

When $n = 2$, p is necessarily equal to 1, and that corresponds to $\theta = 1/2$. So $d_1 = 1 - R_*$ and $d_2 = 1 + R_*$. The construction of the polynomial $\mu_2^{R_*}(\lambda)$ is made as follows. The system (36) gives

$$U^2 + U^0 + (\lambda d_1 - 2)U^1 = 0, \quad U^3 + U^1 + (\lambda d_2 - 2)U^2 = 0,$$
$$U^4 + U^2 + (\lambda d_1 - 2)U^3 = 0.$$

Expressing U^1 in terms of U^0 and U^2 from the first equation, U^3 in terms of U^2 and U^4 from the third equation, and inserting these expressions into the second equation, we obtain

$$U^4 + U^0 + \big(2 - (\lambda d_1 - 2)(\lambda d_2 - 2)\big)U^2 = 0,$$

from which we deduce the polynomial:

$$\mu_2^{R_*}(\lambda) = -(1 - {R_*}^2)\lambda^2 + 4\lambda.$$

Therefore, introducing the three critical values of λ, $\lambda_1^{\pm}(R_*)$ and $\lambda_2(R_*)$, by

$$\lambda_1^{\pm}(R_*) = \frac{2}{1 \mp |R_*|}, \quad \lambda_2(R_*) = \frac{4}{1 - {R_*}^2}, \tag{38}$$

the condition $0 \le \mu_2^{R_*}(\lambda) \le 4$ for the existence of periodic solutions for the system reads as:

$$\begin{cases} \text{when } |R_*| \neq 1, & \lambda \in \left[0, \lambda_1^-(R_*)\right] \cup \left[\lambda_1^+(R_*), \lambda_2(R_*)\right] \\ \text{when } |R_*| = 1, & \lambda \in [0,1]. \end{cases} \tag{39}$$

The case $|R_*| = 1$ is singular and must be treated independently. Note that the interval $\left[\lambda_1^+(R_*), \lambda_2(R_*)\right]$ is on the negative real half-line when $|R_*| > 1$. So, except when $|R_*| = 1$, the original interval of admissibility $[0,4]$ for the 1-periodic system (when $R_* = 0$) is divided into two parts for the 2-periodic system. The first interval, namely $[0, 2/(1 + |R_*|)]$, which is always in the positive real half-line, has a width that progressively decreases from 2 to 0 when $|R_*|$ grows from 0 to ∞. The second interval, $[2/(1 - |R_*|), 4/(1 - {R_*}^2)]$, is split into two branches, progressively rejected to plus or minus infinity when $|R_*|$ tends to 1 from below or from above, respectively. The width of the two branches of this second pass band is monotonically decreasing from 2 to 0 when $|R_*|$ grows from 0 to ∞, see Fig. 10(left).

When $n = 4$, since the case $p = 2$ corresponds to $\theta = 1/2$ treated above, it suffices to consider the case $p = 1$ that corresponds to $\theta = 1/4$. The construction of the polynomial of degree 4 in λ is made in Comi et al. (2025) for a general family of d_i's and gives

$$\mu_4(\lambda) = -d_1 d_2 d_3 d_4 \lambda^4 + c_3 \lambda^3 - c_2 \lambda^2 + 4(d_1 + d_2 + d_3 + d_4)\lambda$$

with $c_3 = 2(d_1 d_2 d_3 + d_2 d_3 d_4 + d_3 d_4 d_1 + d_4 d_1 d_2)$ and $c_2 = 3(d_1 d_2 + d_2 d_3 + d_3 d_4 + d_4 d_1) + 4(d_1 d_3 + d_2 d_4)$. Here

$$d_1 = d_3 = 1, \quad d_2 = 1 - R_*, \quad d_4 = 1 + R_*, \tag{40}$$

and the polynomial reads

$$\mu_4^{R_*}(\lambda) = \lambda(\lambda - 2)^2 \left(1 - (1 - {R_*}^2)\lambda\right). \tag{41}$$

Note that the polynomial is symmetric in R_* and hence the behavior of the system depends only on $|R_*|$. The polynomial passes through 0 when $\lambda = 0$ and when $\lambda = \lambda_4(R_*) := 1/(1 - {R_*}^2)$. Note that $\lambda = 2$ is a double root but the polynomial does not cross $\mu = 0$ at that point because of our choice (40) of the d_i's. It passes through 4 when $\lambda = \lambda_1^{\pm}(R_*)$ or $\lambda_3^{\pm}(R_*)$ with

$$\begin{cases} \lambda_1^{\pm}(R_*) = \dfrac{2 \mp |R_*| - \sqrt{2 \mp 2|R_*| + {R_*}^2}}{1 \mp |R_*|} \\ \lambda_3^{\pm}(R_*) = \dfrac{2 \mp |R_*| + \sqrt{2 \mp 2|R_*| + {R_*}^2}}{1 \mp |R_*|}. \end{cases}$$

Therefore the condition for the existence of periodic solutions reads now as

$$\lambda \in \left[0, \lambda_1^-(R_*)\right] \cup \left[\lambda_1^+(R_*), \lambda_3^-(R_*)\right] \cup \left[\lambda_3^+(R_*), \lambda_4(R_*)\right], \tag{42}$$

when $|R_*| \neq 1$. So the interval of admissibility $[0,4]$ for the 1-periodic system (when $R_* = 0$) is divided into three parts for the 4-periodic system, see Fig. 10(right). Let us note that the third interval, namely $[\lambda_3^+(R_*), \lambda_4(R_*)]$, is in the negative real half-line when $|R_*| > 1$. Outside those parts, there are band-gaps (in terms of λ). Thus, by comparison to the 1-periodic system, new band-gaps start at the double roots of the equation $\mu_4^0(\lambda) = 4$ (μ_4^0 being the polynomial when $R_* = 0$), namely at $\lambda_1^0 = 2 - \sqrt{2}$ and $\lambda_3^0 = 2 + \sqrt{2}$, with a width that progressively increases from 0 to $(\sqrt{5} - 1)/2$ for the first and becomes infinite for the second. The fact that no band-gap appears at $\lambda = 2$ is due to the specific expression (40) that the d_i's have in the present case. The first pass-band $[0, \lambda_1^-(R_*)]$ has a width that progressively decreases from $2 - \sqrt{2}$ to 0 when $|R_*|$ grows from 0 to ∞. Similarly, the width of the second pass-band $[\lambda_1^+(R_*), \lambda_3^-(R_*)]$ decreases from $2\sqrt{2}$ to 0. The third pass-band $[\lambda_3^+(R_*), \lambda_4(R_*)]$ is progressively rejected to infinity with a width that decreases from $2 - \sqrt{2}$ to 0 when $|R_*|$ grows from 0 to 1; then, when $|R_*|$ grows from 1 to ∞, the pass-band goes from $-\infty$ to 0 with a width which starts and finishes at 0, taking its maximal value 0.122 at $|R_*| \approx 3.62$.

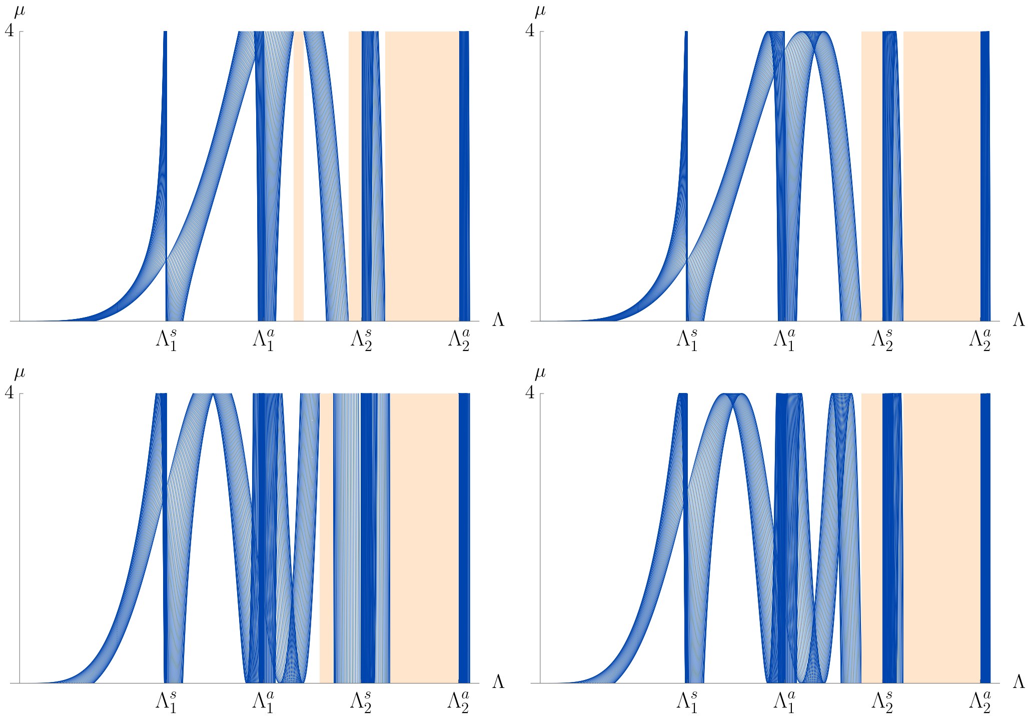

Fig. 11. For $\lambda_0 = 0.01$ and $\mu_0 = 1$, how the quasi-periodicity modifies the domain of admissibility of the frequency Λ where the system admits bounded solution: (up left) when $\theta = 1/2$ and $R = 1/3$; (up right) when $\theta = 1/2$ and $R = 0$ (equivalent to the 1-periodic case); (down left) when $\theta = 1/4$ and $R = 1/2$; (down right) when $\theta = 1/4$ and $R = 0$ (equivalent to the 1-periodic case). (For interpretation of the references to color in this figure legend, the reader is referred to the web version of this article.)

The modifications of the position of the band-gaps due to the loss of the 1-periodicity of the system are shown in Fig. 11 when $\theta = 1/2$ and $R = 1/3$ (up), or $\theta = 1/4$ and $R = 1/2$ (down). In both cases, $\lambda_0 = 0.01$ and $\mu_0 = 1$. The position of the band-gaps for the n-periodic system (when $n = 2$ or 4 with $R \neq 0$) are represented on the left sub-figures and compared with that of the 1-periodic system ($R = 0$) represented in the right sub-figures. In each sub-figure, the evolution with Λ of $\mu = \mu_n^{R_*}(\hat{\lambda}(\kappa, \Lambda))$ is plotted for all values of $\kappa \in [0, \pi]$ (note that the blue regions are the collection of the curves obtained with different discrete values of $\kappa \in [0, \pi]$). The band-gaps, shaded in light orange, correspond to the intervals of Λ for which μ is not in the interval $(0, 4)$. Note that the right sub-figures are not the same because the polynomial $\mu_2^0(\lambda)$ and $\mu_4^0(\lambda)$ are different, but they give the same positions of the band-gaps as expected, since both correspond to the same fully periodic system.

For $\theta = 1/2$, one can see that the two band-gaps of the 1-periodic system located in the intervals $(\Lambda_1^a, \Lambda_2^s]$ and $(\Lambda_2^s, \Lambda_2^a]$ still exist when $R = 1/3$ but their widths are smaller. Specifically, they change from $(5.163, \Lambda_2^s \approx 5.498]$, $(5.839, \Lambda_2^a \approx 7.069]$ to $(5.290, 5.498]$, $(5.883, 7.069]$. On the other hand, a new band-gap appears in the interval $(\Lambda_1^a, \Lambda_2^s]$, namely the interval $(4.409, 4.565)$ when $R = 1/3$ which does not exist when $R = 0$. Thus, the loss of 1-periodicity can both decrease the width of the original band-gaps and create new band-gaps. This trend is confirmed for $\theta = 1/4$. Indeed, the band-gap located in the interval $(\Lambda_2^s, \Lambda_2^a]$ changes from $(5.839, 7.069]$ to $(5.970, 7.069]$ when R changes from 0 to $1/2$, so its width decreases. In the interval $(\Lambda_1^a, \Lambda_2^s]$, when $R = 1/2$ the original band-gap $(5.163, 5.498]$ disappears and is replaced by the band-gap $(4.839, 5.050)$ that does not exist when $R = 0$ and does not close at Λ_2^s. Therefore, the 4-periodicity instead of the 1-periodicity has decreased the width of a band-gap, canceled another one and created a new one in the interval $[0, \Lambda_2^a]$.

In conclusion, those examples show that the replacement of the 1-periodicity by a n-periodicity (and hence by a quasi-periodicity) can have complex and antagonistic effects in terms of pass-bands and band-gaps.

4.2. *Some properties in the general case*

For arbitrary values of n, it is not possible to construct explicitly the polynomial $\mu_n^{R_*}$ because it is defined by induction. However, it is possible to obtain general properties when the parameter R_* is small by using asymptotic methods. Indeed, one can expand then the polynomial in powers of R_*:

$$\mu_n^{R_*}(\lambda) = \mu_n^0(\lambda) + R_* \mu_n^1(\lambda) + {R_*}^2 \mu_n^2(\lambda) + \cdots$$

The polynomial μ_n^0, which corresponds to the 1-periodic system, is known and reads as $\mu_n^0(\lambda) = 2(1 - \cos n\beta)$ when $\lambda \in [0, 4]$, where $\beta \in [0, \pi]$ is defined by $\lambda = 2(1 - \cos\beta)$. Its values enter in the interval $[0, 4]$ at $\lambda = \lambda_0^0 := 0$ and leave it at $\lambda = \lambda_n^0 := 4$. In-between, it oscillates between 0 and 4 reaching these extrema values at $\lambda_I^0 = 2(1 - \cos I\pi/n)$ corresponding to $\beta_I = I\pi/n$, $1 \leq I \leq n-1$, which are double roots. Consequently, when R_* is small the potential new band gaps can only "nucleate" at those points λ_I^0. It is what happens for $n = 2$ or 4 as one can check in the previous subsection. To determine if a band-gap really appears at one λ_I^0, one must evaluate the value of the expansions of the polynomial at that point. It is first shown in Comi et al. (2025) that $\mu_n^1(\lambda_I^0) = 0$ for $0 \leq I \leq n$ and then that the criterion of nucleation "at the first order" in R_* is given by

$$\text{For } 0 < I < n, \text{ if } (-1)^{I+1} \mu_n^2(\lambda_I^0) \begin{cases} > 0 \\ < 0, \end{cases} \quad \text{then } \begin{cases} \text{nucleation} \\ \text{no nucleation.} \end{cases} \tag{43}$$

When $\mu_n^2(\lambda_I^0) = 0$, the nucleation or not of a band-gap at λ_I^0 will depend on higher terms of the expansion. Moreover, when the condition of nucleation is satisfied, then the new band-gap is, at the first order, centered at λ_I^0 with a width $\bar{\lambda}_I$ given by

$$\bar{\lambda}_I = \frac{4R_*}{n} \sin\beta_I \sqrt{(-1)^{I+1} \mu_n^2(\lambda_I)}. \tag{44}$$

Using the relation of induction giving $\mu_n^{R_*}(\lambda)$, one can calculate the second term μ_n^2 of the expansion which, with our choice of the d_i's, reads as

$$\mu_n^2(\lambda) = -\sum_{J=1}^{n}\sum_{K=1}^{J}\frac{\lambda^2}{\sin^2\beta}\sin(n-J+K)\beta\,\sin(J-K)\beta\cos 2J\frac{p}{n}\pi\cos 2K\frac{p}{n}\pi. \tag{45}$$

So, it is sufficient to calculate the double sum above for $\lambda = \lambda_I^0$. The calculations are not detailed here and the interested reader can find the method used in the supplementary file of Comi et al. (2025). One eventually gets

$$\mu_n^2(\lambda_I^0) = \begin{cases} (-1)^{I+1}\dfrac{n^2}{4}\tan^2\dfrac{I\pi}{2n} & \text{if } I \in \{p, n-p\} \\ 0 & \text{otherwise.}\end{cases} \tag{46}$$

Accordingly, a band-gap really nucleates at λ_p^0 and λ_{n-p}^0, that is conform to the results found for $n = 2$ and $n = 4$. At the first order, one deduces from (44)–(46) that the width of the band-gap is equal to $\lambda_p^0 R_*$ and $\lambda_{n-p}^0 R_*$. (Note that for $n = 2$, since $p = n - p = 1$, the width of the band-gap at $\lambda = \lambda_1^0 = 2$ is double and hence equal to $4R_*$.)

Since the result is valid for any θ rational, one can extend it at any real θ of the interval $(0, 1)$. So we have obtained the following result:

Proposition 3. *For a quasi-periodic system whose d_i are given by $d_i = 1 + R_* \cos 2i\theta\pi$ with $\theta \in (0, 1)$, a band-gap nucleates at $\lambda = 2(1 \pm \cos\theta\pi)$ as soon as $R_* \neq 0$. The width of the band-gap is of the first order in R_* for small R_* and equal to λR_*.*

To find if band-gaps nucleate at the points λ_I^0 with $I \notin \{p, n-p\}$, one must consider higher orders of the expansion. Expanding the polynomial $\mu_n^{R_*}$ up to the fourth order, it is shown in Comi et al. (2025) that band-gaps whose width is of the order of ${R_*}^2$ can nucleate at λ_{2p}^0 and λ_{n-2p}^0, but the number of calculations required to apply this result here is too large to be reproduced in this article.

Since $\mu_n^{R_*}(0)$ is always equal to 0, the half-line $(-\infty, 0)$ is always a band-gap. At the other end, the half-line $(\lambda_n(R_*), +\infty)$ is also a band-gap, $\lambda_n(R_*)$ being the last value of λ where the polynomial leaves the interval $[0, 4]$. If we assume that $\lambda_n(R_*)$ can be expanded with respect to R_* as follows : $\lambda_n(R_*) = 4 + \lambda_n^1 R_* + \cdots$, the condition $\mu_n^{R_*}(\lambda_n(R_*)) = \mu_n^0(4)$ expanded to the first order gives

$$0 = \left(\frac{d\mu_n^0}{d\lambda}(4)\lambda_n^1 + \mu_n^1(4)\right)R_* + \cdots.$$

Since $d\mu_n^0/d\lambda(4) \neq 0$ and $\mu_n^1(4) = 0$, one gets $\lambda_n^1 = 0$. That means that the evolution of the upper-bound of the pass-band is of the second order in R_*, which is in conformity with the results obtained for $n = 2$ or 4 (see the vertical tangent at $\lambda = 4$ on the Figs. 10).

Finally, the dependence of the first order nucleated band-gap on θ can be seen in Fig. 12 when $R_* = 0.1$.

As R_* depends on R and Λ (see eq. (37)), it would remain to interpret the above results in terms of the frequency Λ for small values of the parameter R and for any value of θ. We will not address this point here.

5. Adiabatic pumping in the system homogenized in x

In this section we will show how quasi-periodicity allows to obtain adiabatic pumping of longitudinal waves from one bar to another in the system considered in Section 2.2. For plane waves along x of wavenumber k_x, such that $u_j(x) = U_j \exp(\mathrm{i}k_x x)$, Eq. (21) becomes:

$$(\Omega^2 - k_x^2)U_j - \frac{\epsilon^3}{Ad}\left(U_j(w_j(x) + w_{j-1}(x)) - U_{j+1}w_j(x) - U_{j-1}w_{j-1}(x)\right) = 0. \tag{47}$$

Problem (47) is now very similar to the one of Moscatelli et al. (2024), Comi et al. (2025), with the difference that here the solution depends also on the wavenumber k_x along the direction x. Note that the coefficients depend on x through the out-of-plane thickness:

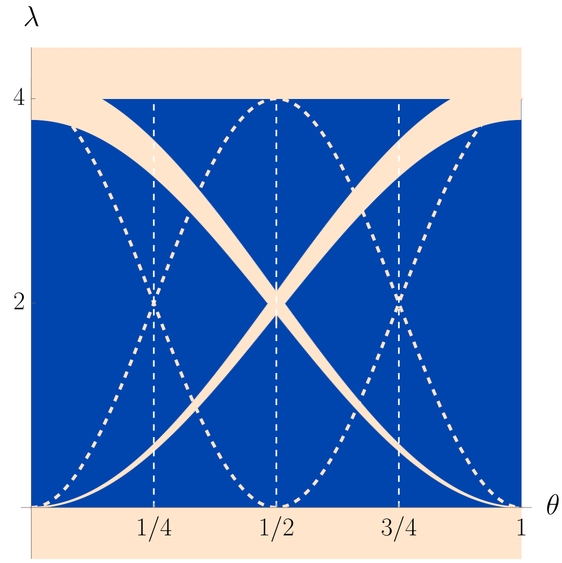

Fig. 12. The light orange domains represent the band-gaps bands on the real line λ estimated by the first-order asymptotic expansion in R_* for $R_* = 0.1$ as a function of $\theta \in (0, 1)$. The orange dotted lines represent where second-order band-gaps bands may appear. (For interpretation of the references to color in this figure legend, the reader is referred to the web version of this article.)

$$w_j(x) = w_0\left[1 + R(\cos(2\pi(\theta x/d + \phi j)))\right] = w_0\tilde{w}_j(x). \tag{48}$$

First, we consider a fixed position x. Problem (47), discrete in y direction with index j, can then be rewritten as:

$$\mu_x^2 U_j - [\tilde{w}_i(U_j - U_{j+1}) + \tilde{w}_{j-1}(U_j - U_{j-1})] = 0, \tag{49}$$

with $\mu_x^2 = (\Omega^2 - k_x^2)\frac{Ad}{\epsilon^3 w_0}$.

When considering a finite number of bars N along direction y, imposing boundary conditions at $j = 0$ and $j = N - 1$, the spectrum of problem (49) is characterized by a finite number of eigenvalues (see Comi et al., 2025; Rosa et al., 2023). Some of these eigenvalues correspond to bulk modes, while others correspond to edge modes, i.e. modes localized at the boundaries $j = 0$ or $j = N - 1$. The latter are positioned at frequencies inside band-gaps of the spectrum of the periodic infinite system obtained by taking as unit cell the finite system under consideration. This is shown for a case where we consider $N = 25$ parallel bars distributed along direction y, with $\hat{\theta}(x) = \theta x/d$, and with parameters $\phi = 1/5$, $R = 2/3$. The infinite periodic system is thus 5-periodic along direction y, with a unit cell varying along x with the phase $\hat{\theta}(x)$. In Fig. 13(a) we show the bulk spectrum of the infinite periodic system by varying $\hat{\theta}$ and the Bloch–Floquet wave number k_y. As expected, five pass-bands, shaded in color, appear in the spectrum due to the periodicity of the system along direction y. In Fig. 13(b), we superimpose the eigenvalues of the finite system with free-free boundary conditions (black curves) over the bulk spectrum of the corresponding infinite system, given by the colored regions in the plot. We find one eigenvalue in each band-gap, corresponding to an edge mode localized at one of the boundaries of the domain.

As expected from the topological properties of the system, these edge modes cross the band-gaps when varying the phase $\hat{\theta}$: an edge mode initially localized at one boundary of the system is transferred to the opposite boundary each time its corresponding curve crosses a band-gap, thus achieving adiabatic pumping of a wave. This is shown in Fig. 14, which displays, in color scale, the absolute value of the displacement field of the edge mode inside the third band-gap of the system governed by Eq. (49), for a varying phase $\hat{\theta}$. The different rows

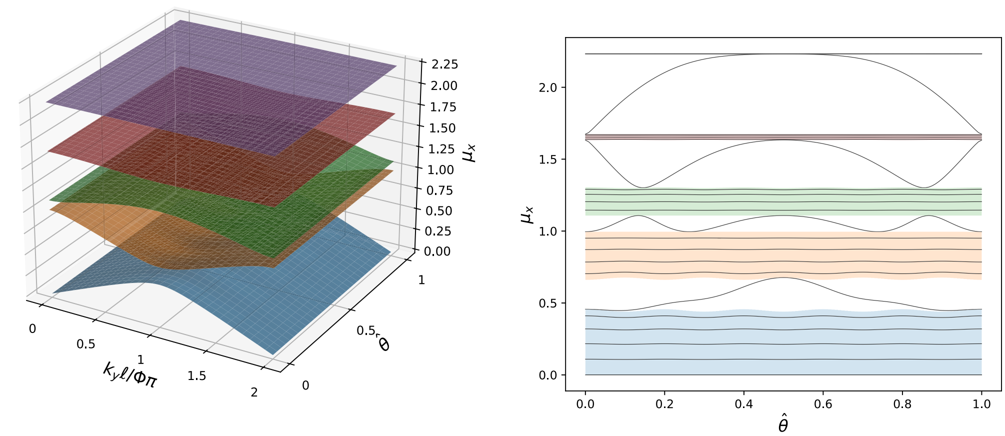

(a) (b)

Fig. 13. (a) Bulk spectrum of the infinite periodic system. (b) Pass-bands of the infinite system (colored regions) and eigenvalues of the finite system with $N = 25$ bars along direction y, for $\phi = 1/5$, and $R = 2/3$ (black lines).

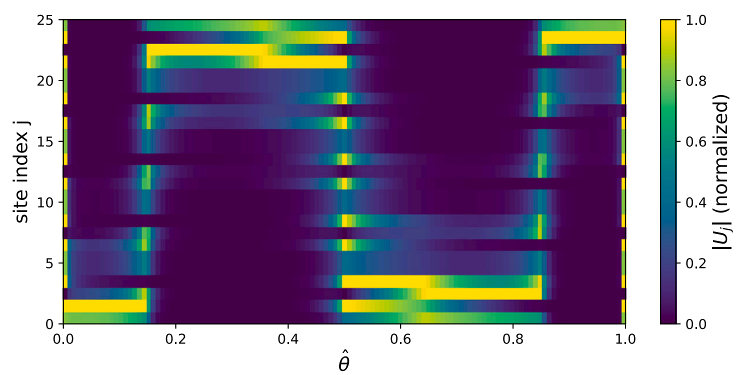

Fig. 14. Adiabatic pumping of an edge mode inside the third band-gap of the system analyzed in Fig. 13b.

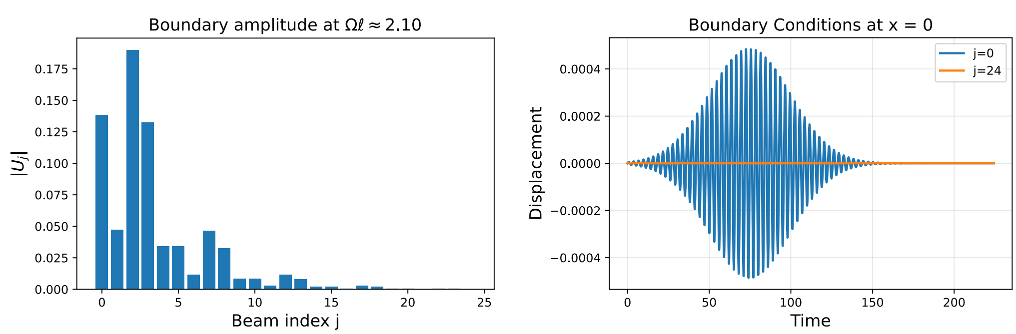

(a) (b)

Fig. 15. (a) Spatial variation of the imposed wave packet at $x = 0$ with $\hat{\theta} = 0.75$. (b) Time variation of the imposed wave packet at $x = 0$ for $j = 0$ (blue line) and $j = N - 1$ (orange line). (For interpretation of the references to color in this figure legend, the reader is referred to the web version of this article.)

correspond to the 25 bars, identified by the index j. From Fig. 13(b), the black curve corresponding to such eigenvalue crosses the band-gap four times. This is in accordance with the results shown in Fig. 14. Initially, the mode is localized in the first bar (i.e. at $j = 0$), at the bottom boundary of the system. By increasing the phase, the mode first moves to the opposite boundary (i.e. at $j = N - 1$), then returns to be localized at the bottom boundary, and finally, it again localizes at the top boundary.

Let us now consider problem (47). The aforementioned adiabatic pumping capabilities have been tested for a two dimensional system with N bars of length L along direction x, at relative distance ℓ in the y direction, by applying to the system the third edge mode at position $x = 0$, as a Gaussian wave packet centered at $\Omega\ell = 2.1$. The imposed signal is shown in Fig. 15, in terms of space variation 15(a) and time variation 15(b), for $j = 0$ (blue line) and $j = N - 1$ (orange line).

The phase $\hat{\theta}$ linearly varies along direction x from 0.75 at $x = 0$, to 1 at $x = L$. According to Fig. 14, the edge mode is expected to move from the bottom boundary ($j = 0$) of the system to the top one ($j = N - 1$). The value for $\Omega\ell$ has been chosen in order to excite propagating waves along the bars. This can be understood by looking at Fig. 16, where we show the dispersion plot in terms of the real and imaginary parts of the wave number k_x, for $\hat{\theta} = 0.75$ which is the phase defining the

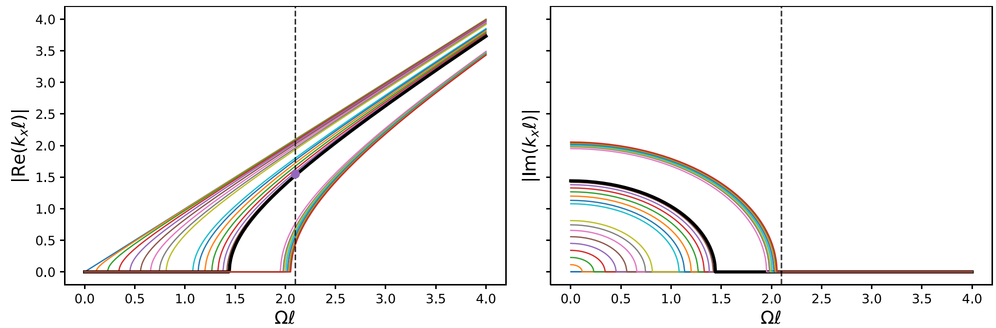

Fig. 16. Dispersion plot for longitudinal waves along the bars: real and imaginary parts of the wavenumber k_x as a function of $\Omega\ell$ for $\hat{\theta} = 0.75$. The bold black line corresponds to the 15-th mode.

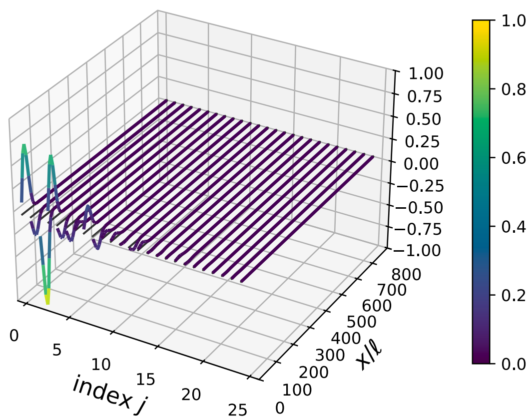

(a) $t = 108$ s

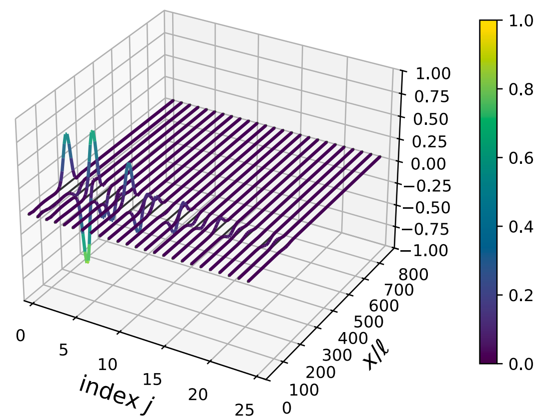

(b) $t = 352$ s

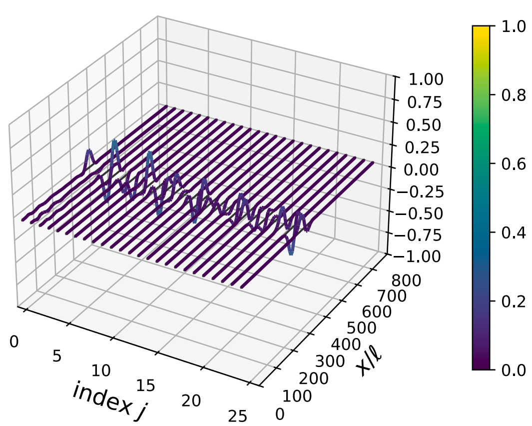

(c) $t = 540$ s

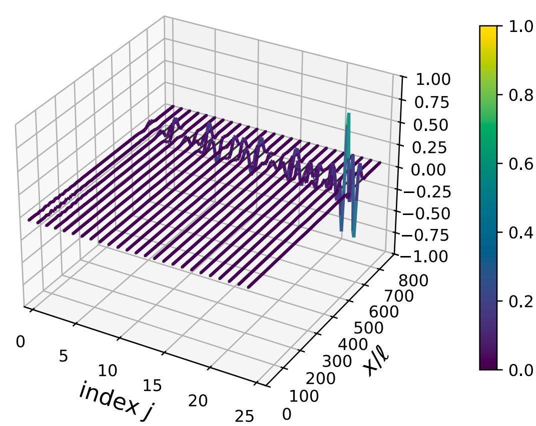

(d) $t = 925$ s

Fig. 17. Response of the system at different time frames, showing the adiabatic pumping of the wave packet from one boundary to the opposite one.

out-of-plane thickness w_j of the elastic connections at $x = 0$. We see from Fig. 16 that for $\Omega\ell = 2.1$ (vertical dashed lines), considering the curve (bold black curve) corresponding to the edge mode inside the third band-gap, i.e. the 15-th mode (see Fig. 13(b)), the system at $x = 0$ indeed supports propagating waves. This can be extended for all positions $x \in [0, L]$, namely to all values of $\hat{\theta}$ used in the system. Note that L has to be chosen sufficiently large to ensure enough space for the pumping to take place and to guarantee a smooth variation of the phase $\hat{\theta}$ after the discretization of the bars used for the forthcoming numerical simulation. Here we take $L = 800\ell$.

The longitudinal displacements of the bars, computed through the inverse Fourier transform, are shown in Fig. 17, for different time frames. The problem is solved using the spectral finite element method, with 40 finite elements along each bar (this number is sufficient to ensure convergence). Note that non-radiating boundary conditions are applied at $x = L$. The details of the numerical implementation are reported in Appendix B. It is clear from the figure that the wave packet is indeed pumped from one boundary of the system to the opposite one, confirming thus the possibility to achieve adiabatic pumping of a wave in the quasi-periodic system under consideration.

6. Conclusions

We studied longitudinal wave propagation in a two-dimensional bar-and-beam lattice with Aubry–André–Harper modulation of the connecting beams, covering both periodic and quasi-periodic arrangements. Starting from the continuous formulation of Helmholtz equation along the bars, we derived a discrete model and established new, fully analytical criteria for the existence of bounded solutions and the nucleation of band-gaps in the limit of a period arrangement. We formulated and demonstrated Proposition 1 proving, for the 2D periodic lattice, the existence of an infinite number of band-gaps occurring starting from sufficiently high frequencies. Then we considered the effect of the loss of periodicity in one direction. The analysis shows that quasi-periodicity, in the context of two-dimensional lattice structures, can both shrink existing band-gaps and create new ones, with their position and width governed by the modulation parameters. These new results show that the behavior of two-dimensional quasi-periodic lattices is different and more complex of that of one-dimensional ones, where the quasi-periodicity leads to nucleation of new band-gaps without altering the ones of the periodic arrangement. The obtained results provide quantitative guidelines to design elastic lattices with tailored longitudinal wave filtering and transport. The loss of periodicity in the other direction is tackled by considering a homogenized problem which can be solved numerically. A specific problem with a finite number of bars is solved, showing that, when properly designed, the system can sustain adiabatic pumping.

Further developments could include the extension of the analysis to flexural waves, and the quantitative assessment of the topological properties in the quasi-periodic setting. Moreover, the lattice system here addressed could be used to study the effect of simultaneous quasi-periodicity in both directions x and y. This study would constitute an interesting extension of the present work.

As shown in Remark 2, under some simplifying assumptions the wave propagation problem in the considered structure is governed by Mathieu equation, which is known to have a rich spectrum of solutions. The discussion of these solutions will be pursued elsewhere.

CRediT authorship contribution statement

Claudia Comi: Writing – review & editing, Writing – original draft, Methodology, Conceptualization. **Marco Moscatelli:** Writing – review & editing, Writing – original draft, Methodology, Conceptualization. **Jean-Jacques Marigo:** Writing – review & editing, Writing – original draft, Methodology, Conceptualization.

Declaration of competing interest

The authors declare that they have no known competing financial interests or personal relationships that could have appeared to influence the work reported in this paper.

Appendix A. Proof of Proposition 1

Let us first establish some properties of the function $\hat{\lambda}$ defined in (30) which can also read as

$$\hat{\lambda}(\kappa,\Lambda)=\lambda_0\Big(\frac{\mu_0}{2}\Lambda^4+F(\Lambda)-\big(F(\Lambda)+G(\Lambda)\big)\sin^2\frac{\kappa}{2}\Big).$$

1. For a given $\kappa\in(0,\pi)$, $\hat{\lambda}(\kappa,\Lambda)$ is not defined when Λ corresponds to a frequency of resonance of the bent beams, but is continuous and monotonically increasing in each interval $(\Lambda^a_{I-1},\Lambda^s_I)$ and $(\Lambda^s_I,\Lambda^a_I)$ for $i\in\mathbb{N}^*$ because F is continuous and increasing while G is continuous and decreasing in those intervals.
2. For $\kappa=0$, $\hat{\lambda}(0,\Lambda)$ is not defined when $\Lambda=\Lambda^s_I$ with $I\in\mathbb{N}^*$. Moreover, $\hat{\lambda}(0,\Lambda)$ increases continuously from 0 to $+\infty$ when Λ grows from 0 to Λ^s_1, and from $-\infty$ to $+\infty$ when Λ grows from Λ^s_I to Λ^s_{I+1} for $I\in\mathbb{N}^*$. Therefore, there exists in each interval $(\Lambda^s_I,\Lambda^s_{I+1})$ with $I\in\mathbb{N}^*$ a unique Λ, denoted $\Lambda^-_{2I+1}(0)$, such that $\hat{\lambda}(0,\Lambda)=0$ and a unique Λ, denoted $\Lambda^+_{2I+1}(0)$, such that $\hat{\lambda}(0,\Lambda)=4$. Moreover, one sets $\Lambda^-_0(0)=0$ and denotes by $\Lambda^+_0(0)$ the unique $\Lambda\in(0,\Lambda^s_1)$ such that $\hat{\lambda}(0,\Lambda)=4$. Thus, one has
$$0=\Lambda^-_0(0)<\Lambda^+_0(0)<\cdots<\Lambda^s_I<\Lambda^-_{2I+1}(0)<\Lambda^+_{2I+1}(0)<\Lambda^s_{I+1}<\cdots.$$
3. For $\kappa=\pi$, $\hat{\lambda}(\pi,\Lambda)$ is not defined when $\Lambda=\Lambda^a_I$ with $I\in\mathbb{N}^*$. Moreover, $\hat{\lambda}(\pi,\Lambda)$ increases continuously from $-3\lambda_0/2<0$ to $+\infty$ when Λ grows from 0 to Λ^a_1, and from $-\infty$ to $+\infty$ when Λ grows from Λ^a_I to Λ^a_{I+1} for $I\in\mathbb{N}^*$. Therefore, there exists in each interval $(\Lambda^a_I,\Lambda^a_{I+1})$ with $I\in\mathbb{N}$ a unique Λ, denoted $\Lambda^-_{2I}(\pi)$, such that $\hat{\lambda}(\pi,\Lambda)=0$ and a unique Λ, denoted $\Lambda^+_{2I}(\pi)$, such that $\hat{\lambda}(\pi,\Lambda)=4$. Thus, one has
$$0<\Lambda^-_0(\pi)<\Lambda^+_0(\pi)<\cdots<\Lambda^a_I<\Lambda^-_{2I}(\pi)<\Lambda^+_{2I}(\pi)<\Lambda^a_{I+1}<\cdots.$$

Let us discuss now the location of possible pass-bands and band gaps in each interval considered in the statement of the Proposition. The discussion is essentially the same for all the intervals and hence we simply detail the arguments for the first interval.

• *In* $[0,\Lambda^s_1]$. For any given $\kappa\in(0,\pi)$, $\hat{\lambda}(\kappa,\Lambda)$ increases continuously from $-\frac{3}{2}\lambda_0\sin^2\frac{\kappa}{2}$ to $+\infty$ when Λ grows from 0 to Λ^s_1. Therefore, there exists a unique $\Lambda^-_0(\kappa)\in(0,\Lambda^s_1)$ such that $\hat{\lambda}(\kappa,\Lambda^-_0(\kappa))=0$, and a unique $\Lambda^+_0(\kappa)\in(0,\Lambda^s_1)$ such that $\hat{\lambda}(\kappa,\Lambda^+_0(\kappa))=4$. Moreover, for any given $\Lambda\in(0,\Lambda^s_1)$, $\kappa\mapsto\hat{\lambda}(\kappa,\Lambda)$ is monotonically decreasing on $(0,\pi)$ because $F(\Lambda)+G(\Lambda)>0$. Then, we obtain the following properties:

(i) $\kappa\mapsto\Lambda^\pm_0(\kappa)$ *is continuously increasing on* $(0,\pi)$.
Proof. The continuity comes from the continuity of $(\kappa,\Lambda)\mapsto\hat{\lambda}(\kappa,\Lambda)$ on $(0,\pi)\times(0,\Lambda^s_1)$. For proving the monotonicity, let us consider $0<\kappa_1<\kappa_2<\pi$. Then, one gets by virtue of the monotonicity of $\kappa\mapsto\hat{\lambda}(\kappa,\Lambda)$:
$$\hat{\lambda}(\kappa_1,\Lambda^\pm_0(\kappa_1))=\hat{\lambda}(\kappa_2,\Lambda^\pm_0(\kappa_2))<\hat{\lambda}(\kappa_1,\Lambda^\pm_0(\kappa_2)),$$
from which one deduces that $\Lambda^\pm_0(\kappa_2)>\Lambda^\pm_0(\kappa_1)$ because of the monotonicity of $\Lambda\mapsto\hat{\lambda}(\kappa,\Lambda)$. □

(ii) $\lim_{\kappa\to0}\Lambda^-_0(\kappa)=\Lambda^-_0(0)=0$ *and*
$$\lim_{\kappa\to\pi}\Lambda^-_0(\kappa)=\Lambda^-_0(\pi)<\lim_{\kappa\to\pi}\Lambda^+_0(\kappa)\le\Lambda^s_1.$$
Proof. The limits exist by virtue of the monotonicity of $\kappa\mapsto\Lambda^\pm_0(\kappa)$. Since $\hat{\lambda}$ is continuous in $[0,\pi]\times[0,\Lambda^s_1)$, we can pass to the limit in $\hat{\lambda}(\kappa,\Lambda^-_0(\kappa))=0$ when κ tends to 0 or π. Then $\hat{\lambda}(0,\lim_{\kappa\to0}\Lambda^-_0(\kappa))=0$ which gives $\lim_{\kappa\to0}\Lambda^-_0(\kappa)=0$. In the same manner, $\hat{\lambda}(\pi,\lim_{\kappa\to\pi}\Lambda^-_0(\kappa))=0$ gives $\lim_{\kappa\to\pi}\Lambda^-_0(\pi)=\Lambda^-_0(\pi)$. For $\kappa\in(0,\pi)$, the strict inequalities $\Lambda^-_0(\kappa)<\Lambda^+_0(\kappa)<\Lambda^s_1$ comes from the monotonicity of $\Lambda\mapsto\hat{\lambda}(\kappa,\Lambda)$ and the definitions of $\Lambda^\pm_0(\kappa)$. By passing to the limits when κ goes to π, we obtain large inequalities, but the equality $\Lambda^-_0(\pi)=\lim_{\kappa\to\pi}\Lambda^+_0(\kappa)$ is not possible because that would lead to
$$0=\hat{\lambda}(\pi,\Lambda^-_0(\pi))=\lim_{\kappa\to\pi}\hat{\lambda}(\kappa,\Lambda^+_0(\kappa))=4,$$
a contradiction. □

(iii) $[0,\Lambda^+_0(\pi)]$ *is a pass-band.*
Proof. By continuity and monotonicity of $\kappa\mapsto\Lambda^-_0(\kappa)$, the interval $[0,\Lambda^-_0(\pi)]$ is a pass-band. By definition of $\Lambda^\pm_0(\pi)$ and by continuity and monotonicity of $\Lambda\mapsto\hat{\lambda}(\pi,\Lambda)$ in $[0,\Lambda^a_1)$, the interval $[\Lambda^-_0(\pi),\Lambda^+_0(\pi)]$ is a pass-band. □

(iv) *If* $\hat{\lambda}(\pi,\Lambda^s_1)\le4$, *then* $[0,\Lambda^s_1]$ *is a pass-band.*
Indeed, if $\hat{\lambda}(\pi,\Lambda^s_1)\le4$, then $\Lambda^+_0(\pi)\ge\Lambda^s_1$ because of the monotonicity of $\Lambda\mapsto\hat{\lambda}(\pi,\Lambda)$, and the result follows from the previous property.

(v) *If* $\hat{\lambda}(\pi, \Lambda_1^s) > 4$, *then* $\Lambda_0^+(\pi) < \Lambda_1^s$ *and* $(\Lambda_0^+(\pi), \Lambda_1^s]$ *is a band-gap.* Proof. If $\hat{\lambda}(\pi, \Lambda_1^s) > 4$, then $\Lambda_0^+(\pi) < \Lambda_1^s$ because of the monotonicity of $\Lambda \mapsto \hat{\lambda}(\pi, \Lambda)$. Moreover $\hat{\lambda}(\kappa, \Lambda) > 4$ for all $\kappa \in [0, \pi]$ and all $\Lambda \in (\Lambda_0^+(\pi), \Lambda_1^s)$, hence this latter interval is a band-gap. Since $\hat{\lambda}(\pi, \Lambda_1^s) > 4$ and $\hat{\lambda}(\kappa, \Lambda_1^s)$ is not defined for $\kappa \in [0, \pi)$, Λ_1^s is also in the band-gap. □

So, we have obtained the result given in the statement of the Proposition with $\Lambda_0 = \Lambda_0^+(\pi)$.

• *In* $(\Lambda_I^s, \Lambda_I^a]$ with I in $\mathbb{N}^*$. For any given $\kappa \in (0, \pi)$, $\hat{\lambda}(\kappa, \Lambda)$ increases continuously from $-\infty$ to $+\infty$ when Λ grows from Λ_I^s to Λ_I^a. Therefore, there exists a unique $\Lambda_{2I+1}^-(\kappa) \in (\Lambda_I^s, \Lambda_I^a)$ such that $\hat{\lambda}(\kappa, \Lambda_{2I+1}^-(\kappa)) = 0$, and a unique $\Lambda_{2I+1}^+(\kappa) \in (\Lambda_I^s, \Lambda_I^a)$ such that $\hat{\lambda}(\kappa, \Lambda_{2I+1}^+(\kappa)) = 4$. Moreover, for any given $\Lambda \in (\Lambda_I^s, \Lambda_I^a)$, $\kappa \mapsto \hat{\lambda}(\kappa, \Lambda)$ is monotonically increasing on $(0, \pi)$ because $F(\Lambda) + G(\Lambda) < 0$. Then, we obtain the following properties by arguments similar to those used for the interval $[0, \Lambda_1^s]$:

(i) $\kappa \mapsto \Lambda_{2I+1}^{\pm}(\kappa)$ *is continuously decreasing on* $(0, \pi)$. (Essentially because $\kappa \mapsto \hat{\lambda}(\kappa, \Lambda)$ is monotonically increasing on $(0, \pi)$ when $\Lambda \in (\Lambda_I^s, \Lambda_I^a)$.)

(ii) $\lim_{\kappa \to \pi} \Lambda_{2I+1}^-(\kappa) = \Lambda_I^s$ *and*

$$\lim_{\kappa \to 0} \Lambda_{2I+1}^-(\kappa) = \Lambda_{2I+1}^-(0) < \lim_{\kappa \to 0} \Lambda_{2I+1}^+(\kappa) \le \Lambda_I^a.$$

(iii) $(\Lambda_I^s, \Lambda_{2I+1}^+(0)]$ *is a pass-band.*

(iv) *If* $\hat{\lambda}(0, \Lambda_I^a) \le 4$, *then* $(\Lambda_I^s, \Lambda_I^a]$ *is a pass-band.*

(v) *If* $\hat{\lambda}(0, \Lambda_I^a) > 4$, *then* $\lim_{\kappa \to 0} \Lambda_{2I+1}^+(\kappa) = \Lambda_{2I+1}^+(0) < \Lambda_I^a$ *and* $(\Lambda_{2I+1}^+(0), \Lambda_I^a]$ *is a band-gap.*

So, we have obtained the result given in the statement of the Proposition with $\Lambda_{2I+1} = \Lambda_{2I+1}^+(0)$.

• *In* $(\Lambda_I^a, \Lambda_{I+1}^s]$ with I in $\mathbb{N}^*$. The discussion is essentially the same as for the interval $[0, \Lambda_1^s]$. The unique difference is that the frequency Λ_I^a is not considered here, but in the previous interval.

Appendix B. Numerical solution details

Problem (21) can be rewritten in matrix form as:

$$\{u\}'' + \Omega^2\{u\} - [\Gamma]\{u\} = \{0\}, \tag{B.1}$$

where $\{u\} = \{u_0(x), u_1(x), \dots, u_{N-1}(x)\}^T$ is the vector of displacements along each bar, N is the number of bars in y direction and the matrix $[\Gamma]$ reads

$$[\Gamma] = \frac{\epsilon^3 w_0}{Ad}\begin{bmatrix} \tilde{w}_0 & -\tilde{w}_0 & 0 & \cdots & \cdots & 0 \\ -\tilde{w}_0 & \tilde{w}_0 + \tilde{w}_1 & -\tilde{w}_1 & \ddots & & \vdots \\ 0 & -\tilde{w}_1 & \tilde{w}_1 + \tilde{w}_2 & \ddots & & \vdots \\ \vdots & \ddots & -\tilde{w}_{j-1} & \tilde{w}_{j-1} + \tilde{w}_j & -\tilde{w}_j & \vdots \\ \vdots & & & \ddots & \ddots & \vdots \\ 0 & \cdots & \cdots & 0 & -\tilde{w}_{N-2} & \tilde{w}_{N-2} \end{bmatrix}. \tag{B.2}$$

To solve the above problem, let us first solve for a fixed position x the eigenvalue problem associated to the matrix $[\Gamma]$, with free-free boundary conditions in the y direction. Note that $[\Gamma]$ is a tridiagonal symmetric matrix, thus all its eigenvalues are real and its eigenvectors are orthogonal. We denote by ν^m, with $m = \{0, \dots, N-1\}$, the eigenvalues. Accordingly, the displacement vector can be expressed as a linear combination of the eigenmodes, namely

$$\{u\} = [\psi]\{q\}, \tag{B.3}$$

where $\{q\} = \{q_0(x), q_1(x), \dots, q_{N-1}(x)\}^T$ is the vector of modal coordinates, and $[\psi]$ is the matrix whose columns are made up of the N orthonormal eigenmodes of $[\Gamma]$. Substituting the expression (B.3) in Eq. (B.1), we obtain

$$[\psi]\{q\}'' + \Omega^2[\psi]\{q\} - [\Gamma][\psi]\{q\} = \{0\}. \tag{B.4}$$

Pre-multiplying the above equation by $[\psi]^T$, and using the orthogonality property of the eigenmodes, we obtain a system of N decoupled differential equations :

$$q_m(x)'' + (\Omega^2 - (\nu^m)^2)q_m(x) = 0, \quad m = \{0, \dots, N-1\}, \tag{B.5}$$

for a fixed coordinate x. Let us consider for a moment that $w_j(x) = w_j$, namely it is constant along the bars, but can vary from one bar to the other. In that case, the general solution of the above equation is :

$$q_m(x) = A_m e^{\mathrm{i}k_x^m x} + B_k e^{-\mathrm{i}k_x^m x}, \tag{B.6}$$

with $k_x^m = \sqrt{\Omega^2 - (\nu^m)^2}$, A_m and B_m being constants to be determined.

Remark 5. Note that the resulting waves are dispersive, with a cut-off frequency for each mode given by $\Omega = \nu^m$. Below this frequency the wavenumber k_x^m is purely imaginary and the wave is evanescent. Accordingly, far enough from the source, only waves at frequencies higher than ν^m will be present.

Let us now consider the general case where $w_j(x)$ varies along each bar. For this, we discretize each rod using N_e finite elements, each one of length a. Within each element, we consider w_j constant and equal to w_j^e in element e, with $e = \{0, \dots, N_e - 1\}$. The general solution (B.6) is thus valid within each element e, with k_x^m now depending also on e.

We first treat each element along direction x separately. In order to combine the information along direction y across all the N bars, let us define the following vectors:

$$\begin{aligned} \{u^0\} &= \{u_0(0), u_1(0), \dots, u_{N-1}(0)\}^T \\ \{u^a\} &= \{u_0(a), u_1(a), \dots, u_{N-1}(a)\}^T \\ \{N^0\} &= -\{N_0(0), N_1(0), \dots, N_{N-1}(0)\}^T \\ \{N^a\} &= \{N_0(a), N_1(a), \dots, N_{N-1}(a)\}^T \end{aligned} \tag{B.7}$$

where u_j and $N_j = EAu_j'$ are the displacement and axial force in bar j, respectively. Note that the index of element e has been dropped for clarity. Using the vector of coefficients $\{C\}$ defined as:

$$\{C\} = \{A_0, B_0, A_1, B_1, \dots, A_{N-1}, B_{N-1}\}^T, \tag{B.8}$$

relations (B.7) can be expressed as :

$$\begin{aligned} \begin{pmatrix} \{u^0\} \\ \{u^a\} \end{pmatrix} &= \underbrace{\begin{bmatrix} [\psi] & [\psi] \\ [\psi]\{e^{-\mathrm{i}Ka}\} & [\psi]\{e^{\mathrm{i}Ka}\} \end{bmatrix}}_{[S]}\{C\}, \\ \begin{pmatrix} \{N^0\} \\ \{N^a\} \end{pmatrix} &= EA\underbrace{\begin{bmatrix} [\psi]\{\mathrm{i}K\} & [\psi]\{-\mathrm{i}K\} \\ [\psi]\{-\mathrm{i}Ke^{-\mathrm{i}Ka}\} & [\psi]\{\mathrm{i}Ke^{\mathrm{i}Ka}\} \end{bmatrix}}_{[R]}\{C\}, \end{aligned} \tag{B.9}$$

where K is a vector containing the k_x^m, with $m = \{0, 1, \dots, N-1\}$. Using relations (B.9), we can eliminate the vector of coefficients $\{C\}$ and obtain the elemental stiffness matrix $[K_e]$ such that :

$$\begin{pmatrix} \{N^0\} \\ \{N^a\} \end{pmatrix} = [K_e]\begin{pmatrix} \{u^0\} \\ \{u^a\} \end{pmatrix}, \tag{B.10}$$

with

$$[K_e] = [R][S]^{-1}. \tag{B.11}$$

The global stiffness matrix $[K]$ can then be obtained assembling the elemental stiffness matrices $[K_e]$, by applying the standard finite element assembly procedure. Finally, by imposing appropriate boundary conditions, the global system can be solved for a given frequency Ω.

Remark 6. Note that the above procedure can be easily adapted to consider different boundary conditions along direction y, by changing the eigenvalue problem associated to matrix $[\Gamma]$.

Remark 7. Non-reflecting boundary conditions are implemented at the right border of the system along direction x, by considering only outgoing waves in the last element. This leads to the following relation between forces and displacements at the right boundary :

$$\{N^L\} = [K_{NR}]\{u^L\}, \tag{B.12}$$

with

$$[K_{NR}] = [\psi]EA\{\mathrm{i}K\}[\psi]^T. \tag{B.13}$$

Remark 8. The problem is solved for each frequency Ω independently. The solution in time is then obtained by applying the inverse Fourier transform.

Data availability

No data was used for the research described in the article.

References

Ammari, H., Davies, B., Hiltunen, E.O., Yu, S., 2020. Topologically protected edge modes in one-dimensional chains of subwavelength resonators. J. Mathématiques Pures Appliquées 144, 17–49. http://dx.doi.org/10.1016/j.matpur.2020.08.007.

Asch, J., Joye, A., Beig, R., Beiglböck, W., Domcke, W., Englert, B.G., Frisch, U., Hänggi, P., Hasinger, G., Hepp, K., Hillebrandt, W., Imboden, D., Jaffe, R.L., Lipowsky, R., Löhneysen, H.V., Ojima, I., Sornette, D., Theisen, S., Weise, W., Wess, J., Zittartz, J. (Eds.), 2006. Mathematical physics of quantum mechanics: Selected and refereed lectures from QMath9. In: Lecture Notes in Physics, vol. 690, Springer, Berlin, Heidelberg, http://dx.doi.org/10.1007/b11573432.

Aubry, S., André, G., 1980. Analyticity breaking and Anderson localization in incommensurate lattices. Ann. Isr. Phys. Soc. 3, 133–165.

Bonnecaze, R.T., Rodin, G.J., Sigmund, O., Søndergaard Jensen, J., 2003. Systematic design of phononic band–gap materials and structures by topology optimization. Philos. Trans. R. Soc. A: Math. Phys. Eng. Sci. 361 (1806), 1001–1019. http://dx.doi.org/10.1098/rsta.2003.1177.

Bordiga, G., Bigoni, D., Piccolroaz, A., 2022. Tensile material instabilities in elastic beam lattices lead to a bounded stability domain. Philos. Trans. R. Soc. A: Math. Phys. Eng. Sci. 380 (2231), 20210388. http://dx.doi.org/10.1098/rsta.2021.0388.

Brillouin, L., 1953. Wave Propagation in Periodic Structures. Dover, New York.

Cabras, L., Bigoni, D., Piccolroaz, A., 2024. Dynamics of elastic lattices with sliding constraints. Proc. R. Soc. A: Math. Phys. Eng. Sci. 480 (2282), 20230579. http://dx.doi.org/10.1098/rspa.2023.0579.

Carrara, M., Cacan, M.R., Toussaint, J., Leamy, M.J., Ruzzene, M., Erturk, A., 2013. Metamaterial-inspired structures and concepts for elastoacoustic wave energy harvesting. Smart Mater. Struct. 22 (6), 065004. http://dx.doi.org/10.1088/0964-1726/22/6/065004.

Chesnais, C., Boutin, C., Hans, S., 2015. Effects of the local resonance in bending on the longitudinal vibrations of reticulated beams. Wave Motion 57, 1–22. http://dx.doi.org/10.1016/j.wavemoti.2015.03.001.

Comi, C., Marigo, J.J., Moscatelli, M., 2025. Some general properties of the band-gap structure for quasi-periodic 1D lattices. Meccanica 60 (8), 2587–2606. http://dx.doi.org/10.1007/s11012-024-01914-y.

Davies, B., Craster, R.V., 2022. Symmetry-induced quasicrystalline waveguides. Wave Motion 115, 103068. http://dx.doi.org/10.1016/j.wavemoti.2022.103068.

Davies, B., Morini, L., 2024. Super band gaps and periodic approximants of generalised Fibonacci tilings. Proc. R. Soc. A: Math. Phys. Eng. Sci. 480 (2285), 20230663. http://dx.doi.org/10.1098/rspa.2023.0663.

De Ponti, J.M., Riva, E., Ardito, R., Braghin, F., Corigliano, A., 2020. Wide low frequency bandgap in imperfect 3D modular structures based on modes separation. Mech. Res. Commun. 105, 103512. http://dx.doi.org/10.1016/j.mechrescom.2020.103512.

Delourme, B., Fliss, S., Joly, P., Vasilevskaya, E., 2016. Trapped Modes in Thin and Infinite Ladder Like Domains: Existence and Asymptotic Analysis. Research Report RR-8882, (CNRS-ENSTA Paristech-INRIA, Université Paris-Saclay) ; LAGA, Université Paris 13.

Faraci, D., Mendicino, F., Vincenti, A., Comi, C., 2023. Wave polarization control in anisotropic locally resonant materials. Appl. Sci. 13 (19), http://dx.doi.org/10.3390/app131910797.

Gei, M., 2010. Wave propagation in quasiperiodic structures: stop/pass band distribution and prestress effects. Int. J. Solids Struct. 47, 3067–3075. http://dx.doi.org/10.1016/j.ijsolstr.2010.07.008.

Guo, Y., Rosa, M.I., Ruzzene, M., 2024. Topological gaps in twist-induced two-dimensional quasiperiodic locally resonant metastuctures. Phys. Rev. Appl. 22, http://dx.doi.org/10.1103/PhysRevApplied.22.064004.

Harper, P.G., 1955. Single band motion of conduction electrons in a uniform magnetic field. Proc. Phys. Soc. Sect. A 68 (10), 874. http://dx.doi.org/10.1088/0370-1298/68/10/304.

Hofstadter, D.R., 1976. Energy levels and wave functions of Bloch electrons in rational and irrational magnetic fields. Phys. Rev. B 14 (6), 2239–2249. http://dx.doi.org/10.1103/PhysRevB.14.2239.

Jiao, P., Mueller, J., Raney, J.R., Zheng, X.R., Alavi, A.H., 2023. Mechanical metamaterials and beyond. Nat. Commun. 14 (1), 6004. http://dx.doi.org/10.1038/s41467-023-41679-8.

Kannan, V., Dorn, C., Drechsler, U., Kochmann, D.M., 2026. Microscale architected materials for elastic waveguiding: Fabrication and dynamic characterization across length and time scales. Phys. Rev. X 16, 011047. http://dx.doi.org/10.1103/21w4-zn1s.

Khelif, A., Deymier, P.A., Djafari-Rouhani, B., Vasseur, J.O., Dobrzynski, L., 2003. Two-dimensional phononic crystal with tunable narrow pass band: Application to a waveguide with selective frequency. J. Appl. Phys. 94 (3), 1308–1311. http://dx.doi.org/10.1063/1.1557776.

Kittel, C., 1953. Introduction to Solid State Physics. Wiley, New York.

Kraus, Y.E., Lahini, Y., Ringel, Z., Verbin, M., Zilberberg, O., 2012. Topological states and adiabatic pumping in quasicrystals. Phys. Rev. Lett. 109 (10), 106402. http://dx.doi.org/10.1103/PhysRevLett.109.106402.

LeGrande, J., Malla, A., Bukhari, M., Barry, O., 2024. Introduction of local resonators to a nonlinear metamaterial with topological features. J. Comput. Nonlinear Dyn. 19, http://dx.doi.org/10.1115/1.4064726.

Lv, H., Tian, X., Wang, M.Y., Li, D., 2013. Vibration energy harvesting using a phononic crystal with point defect states. Appl. Phys. Lett. 102 (3), 2013–2016. http://dx.doi.org/10.1063/1.4788810.

Madine, K.H., Colquitt, D.J., 2022. Negative refraction and mode trapping of flexural-torsional waves in elastic lattices. Philos. Trans. A Math Phys. Eng. Sci. 380 (2237), 20210379. http://dx.doi.org/10.1098/rsta.2021.0379.

Marigo, J.J., Maurel, A., Pham, K., 2023. Negative refraction in a single-phase flexural metamaterial with hyperbolic dispersion. J. Mech. Phys. Solids 170, http://dx.doi.org/10.1016/j.jmps.2022.105126.

Martí-Sabaté, M., Torrent, D., 2021. Edge modes for flexural waves in quasi-periodic linear arrays of scatterers. APL Mater. 9 (8), 081107. http://dx.doi.org/10.1063/5.0059097.

Martínez, A.J., Porter, M.A., Kevrekidis, P.G., 2018. Quasiperiodic granular chains and hofstadter butterflies. Philos. Trans. Ser. A Math. Phys. Eng. Sci. 376 (2127), 20170139. http://dx.doi.org/10.1098/rsta.2017.0139.

Maurel, A., Pham, K., Semblat, J.-F., Félix, S., 2025. Urban seismology: A homogenization perspective on site–city and site–foundation–city interaction. Bull. Seismol. Soc. Am. 116 (2), 535–552. http://dx.doi.org/10.1785/0120250151.

Mead, D., 1970. Free wave propagation in periodically supported, infinite beams. J. Sound Vib. 11 (2), 181–197. http://dx.doi.org/10.1016/S0022-460X(70)80062-1.

Miles, J., 1956. Vibrations of beams on many supports. J. Eng. Mech.-Asce 82, 1–9.

Moscatelli, M., Comi, C., Marigo, J.J., 2020. Energy localization through locally resonant materials. Materials 13 (13), http://dx.doi.org/10.3390/ma13133016.

Moscatelli, M., Comi, C., Marigo, J.J., 2024. Wave transmission in quasi-periodic lattices. Philos. Trans. R. Soc. A: Math. Phys. Eng. Sci. 382 (2279), 20230351. http://dx.doi.org/10.1098/rsta.2023.0351.

Ni, X., Chen, K., Weiner, M., Apigo, D.J., Prodan, C., Alù, A., Prodan, E., Khanikaev, A.B., 2019. Observation of Hofstadter butterfly and topological edge states in reconfigurable quasi-periodic acoustic crystals. Commun. Phys. 2 (1), 55. http://dx.doi.org/10.1038/s42005-019-0151-7.

Palermo, A., Krödel, S., Marzani, A., Daraio, C., 2016. Engineered metabarrier as shield from seismic surface waves. Sci. Rep. 6, 39356. http://dx.doi.org/10.1038/srep39356.

Pu, X., Palermo, A., Marzani, A., 2022. Topological edge states of quasiperiodic elastic metasurfaces. Mech. Syst. Signal Process. 181, http://dx.doi.org/10.1016/j.ymssp.2022.109478.

Rallu, A., Hans, S., Boutin, C., 2018. Asymptotic analysis of high-frequency modulation in periodic systems. analytical study of discrete and continuous structures. J. Mech. Phys. Solids 117, 123–156. http://dx.doi.org/10.1016/j.jmps.2018.04.014.

Rosa, M.I.N., Davis, B.L., Liu, L., Ruzzene, M., Hussein, M.I., 2023. Material vs. structure: Topological origins of band-gap truncation resonances in periodic structures. Phys. Rev. Mater. 7 (12), 124201. http://dx.doi.org/10.1103/PhysRevMaterials.7.124201.

Rosa, M.I., Pal, R.K., Arruda, J.R., Ruzzene, M., 2019. Edge states and topological pumping in spatially modulated elastic lattices. Phys. Rev. Lett. 123, http://dx.doi.org/10.1103/PhysRevLett.123.034301.

Xia, Y., Erturk, A., Ruzzene, M., 2020. Topological edge states in quasiperiodic locally resonant metastructures. Phys. Rev. Appl. 13 (1), 014023. http://dx.doi.org/10.1103/PhysRevApplied.13.014023.